UNIVERSITÀ
DEGLI STUDI
DI PADOVA

DIPARTIMENTO
DI INGEGNERIA
DELL'INFORMAZIONE

DIPARTIMENTO DI INGEGNERIA DELL'INFORMAZIONE

CORSO DI LAUREA MAGISTRALE IN

BIOINGEGNERIA INDUSTRIALE

Direct ink writing of bioactive sphene ceramic scaffolds made of silicone-based emulsions

Relatore: Prof. HAMADA ELSAYED

Correlatore: Prof. ENRICO BERNARDO

Ing. VALERIA DIAMANTI

Laureanda: Maria Giuseppa Guerra

ANNO ACCADEMICO 2023 – 2024

Data di laurea 15 ottobre 2024

“Rimani zitto, niente pareri
Il tuo soffitto, stelle e pianeti
A capofitto nel tuo limbo, in preda ai pensieri
Procedi nel tuo labirinto senza pareti”

Index

Figures Index

Tables Index

Abstract

Throughout the centuries, human beings have always searched among the objects around them for something that could serve to improve their quality-of-life following accidents or congenital malformations.

It is important to remember that the first functional prosthesis, a big toe, can be traced back to the fifth Egyptian dynasty (2750-2625 B.C.), but many things have changed since then.

The choice of random materials did not always prove to be the best option, as the resulting rudimentary prostheses were hardly ever biocompatible, e.g. the use of iron and wood very often caused adverse reactions.

An approach that has become increasingly popular in the last decade concerns tissue engineering, i.e. the design and production of scaffolds integrated with cells that restore tissue function after implantation.

Materials engineering has therefore come to support biomedical engineering by optimizing materials precisely based on the use to which the prosthesis is to be put, as scaffolds must be bioinert, biocompatible and biodegradable and respect the characteristics of the native tissue.

This work aims to obtain titanite, also known as sphene ($CaTiSiO_5$), a bioactive ceramic material due to its ability to interact favourably with biological tissues, particularly bone, promoting bone growth and the formation of tissue bonds.

Bioactivity is linked to its chemical composition and crystalline structure as it contains calcium ions and is found to have better mechanical properties and greater stability than bioglass and calcium phosphate materials.

The innovation of this work concerns the methodology used to obtain sphene, the emulsion between an oily phase based on resin and silicone products and an aqueous phase in which calcium crystals and titanium dioxide are dissolved as fillers.

Mixtures from two calcic precursors were presented: the calcium nitrate tetrahydrate $Ca(NO_3)_2 \cdot 4H_2O$ and calcite $CaCO_3$.

In this work, scaffold moulding was carried out by means of Direct Ink Writing, an Additive Manufacturing technique that is particularly promising in the field of tissue engineering,

which enables the moulding of biological materials as well as the creation of complex structures required for tissue growth and regeneration.

The conversion of the polymer precursor takes place via heat treatment at temperatures between 1300°C and 1350°C.

Following heat treatment, it will then be necessary to assess the composition of the material obtained, comparing the peaks of X-ray diffractometry analyses and characterizing it both mechanically, by performing mechanical compression tests, and physically, by assessing its density and porosity.

Finally, the characterization of the microstructure will be performed by scanning electron microscopy.

Prefazione

Nel corso dei secoli, l'essere umano ha sempre cercato tra gli oggetti che lo circondavano qualcosa che potesse servire a migliorare la qualità della vita in seguito a incidenti o malformazioni congenite.

È importante ricordare che la prima protesi funzionale, un alluce, può essere fatta risalire alla quinta dinastia egizia (2750-2625 a.C.), ma da allora molte cose sono cambiate.

La scelta di materiali casuali non sempre si è rivelata l'opzione migliore, poiché le rudimentali protesi che ne derivavano risultavano quasi mai biocompatibili, ad esempio l'uso del ferro e del legno molto spesso provocavano reazioni avverse.

Un approccio che si sta affermando sempre di più nell'ultimo decennio riguarda l'ingegneria tissutale, ovvero la progettazione e la produzione di impalcature integrate con cellule che ripristinano la funzione dei tessuti dopo l'impianto.

L'ingegneria dei materiali è venuta quindi in supporto dell'ingegneria biomedica andando a ottimizzare i materiali proprio sulla base dell'uso che la protesi dovrà andare a svolgere, in quanto le impalcature devono essere bioinerti, biocompatibili e biodegradabili e rispettare le caratteristiche del tessuto nativo.

Questo lavoro mira a ottenere la titanite, chiamata anche sfene ($CaTiSiO_5$), un materiale ceramico bioattivo per la sua capacità di interagire favorevolmente con i tessuti biologici, in particolare le ossa, promuovendo la crescita ossea e la formazione di legami con i tessuti.

La bioattività è legata alla sua composizione chimica e alla sua struttura cristallina in quanto contiene ioni calcio e risulta avere migliori proprietà meccaniche e maggiore stabilità rispetto ai materiali in biovetro e fosfato di calcio

L'innovazione di questo lavoro riguarda la metodologia utilizzata per ottenere lo sfene, l'emulsione tra una fase oleosa a base di resina e prodotti siliconici e una fase acquosa in cui sono disciolti cristalli di calcio e biossido di titanio come fillers.

Sono state presentate miscele a partire da due precursori calcici: il calcionitrato tetraidrato $Ca(NO_3)_2{\cdot}4H_2O$ e la calcite $CaCO_3$.

In questo lavoro lo stampaggio degli scaffold è stato eseguito mediante Direct Ink Writing, una tecnica di Additive Manufacturing particolarmente promettente nell'ambito

dell'ingegneria tissutale che permette di stampare materiali biologici ma anche di creare strutture complesse necessarie per la crescita e la rigenerazione dei tessuti.

La conversione del precursore polimerico avviene tramite trattamento termico a temperature comprese tra 1300°C e 1350°C.

In seguito al trattamento termico sarà poi necessario valutare la composizione del materiale ottenuto, andando a confrontare i picchi delle analisi di diffrattometria ai raggi X e caratterizzarlo sia meccanicamente, effettuando prove meccaniche a compressione, ma anche fisicamente, valutandone la densità e la porosità.

Infine, la caratterizzazione della microstruttura verrà eseguita tramite microscopia a scansione elettronica.

Chapter 1

Bone Tissue

Bone tissue is a particular type of highly specialised connective tissue, the main purpose of which is to provide the scaffolding capable of supporting and protecting the human body as a whole.

Bone itself is not only able to provide mechanical support and protection for internal organs, but also acts as a reservoir of minerals, such as phosphate and calcium, which can be released and stored due to the dynamic remodelling action to which bone is continuously subjected. Bone is also actively involved in the production of blood cells through the process of haematopoiesis, as bone marrow is contained within it, controlling the production of red blood cells, white blood cells and platelets.

In this chapter, the main characteristics of bone tissue, its structure and biomechanical properties will be explained, analysing its essential role in human physiology.

Structure and Composition

Bone tissue, along with cartilage tissue, is classified as a supporting connective tissue and, like all connective tissues, originates from the mesenchyme, an embryonic connective tissue that in turn originates from the mesoderm.

The fundamental characteristic of bone tissue is the composition of the extracellular matrix; in fact, it is organised into two main components: the organic and inorganic components.

- **Organic component**: constitutes about 33 % of the bone weight and is composed of type I collagen fibres that give the bone tensile strength and flexibility, toughness and elasticity.
- **Inorganic component**: accounts for the remaining 67% and is composed of hydroxyapatite [$Ca_{10}(PO_4)_6(OH)_2$], a crystalline form of calcium phosphate, which, when arranged parallel to the collagen fibres, gives the bone rigidity and compressive strength. [1]

In view of these characteristics, bone tissue is defined as a composite material.

Observing bone tissue under a microscope allows one to assess how it is composed in three-dimensional space.

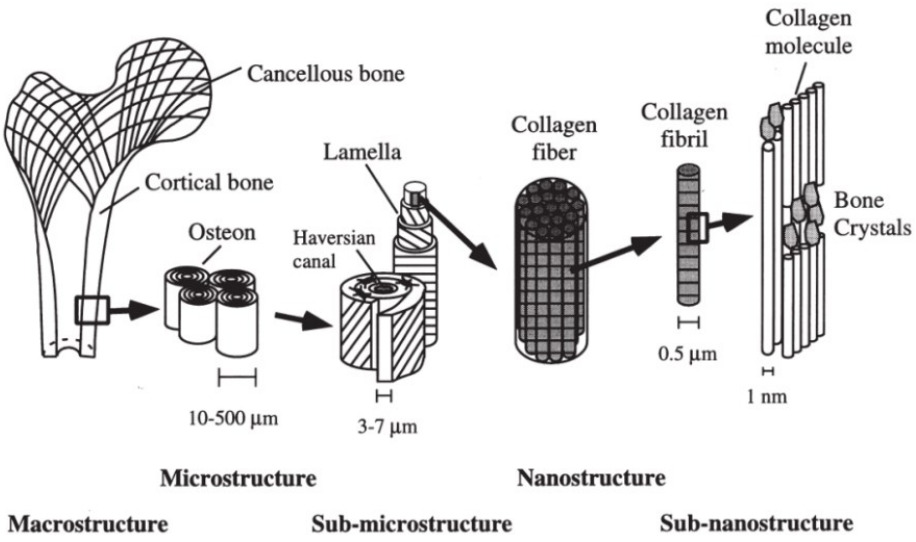

Figure 1: Bone Tissue Components in range 10 µm to 1nm (I)

Three types of bone tissue can be recognised:

- **Fibrous bone tissue**: under normal conditions, this tissue is present in the embryo until neonatal age and during fracture healing.

  This type is more elastic as it has a reduced amount of minerals and an unordered arrangement of collagen fibres.
- **Compact, or cortical, bone tissue** (80% of skeletal mass): located in the outer layer of short, flat bones and in the diaphysis of long bones. It is essential for resistance to shocks and applied mechanical loads.

  The cortical bone is organised in structural units, immersed in an interstitial tissue formed by old osteons and collagen, called osteons or Havers'systems: cylindrical structures formed by concentric lamellae delimiting a central canal called Harves' canal within which blood vessels and nerves run.

  Harves' canals communicate with each other via Volkmann's canals, which have an orthogonal direction to the former. Between the lamellae there are gaps between 10 and 50 µm, in which osteocytes are present.
- **Spongy or trabecular bone** (20 % of the skeletal mass): found mainly in the ends of long bones and inside the short and flat bones. The lamellae are arranged to form the characteristic trabecular structure that makes this tissue light and strong. The spatial organisation of the trabeculae depends on the mechanical conditions applied to the bone structure: the trabeculae will be arranged in such a way as to optimise the structure by improving mechanical strength while minimising weight.

The density and orientation properties of the trabeculae are determined by the optimisation process that varies according to the specific load in each area of the trabecular bone. The medullary cavities, bordered by trabeculae, hold the red and yellow marrow.

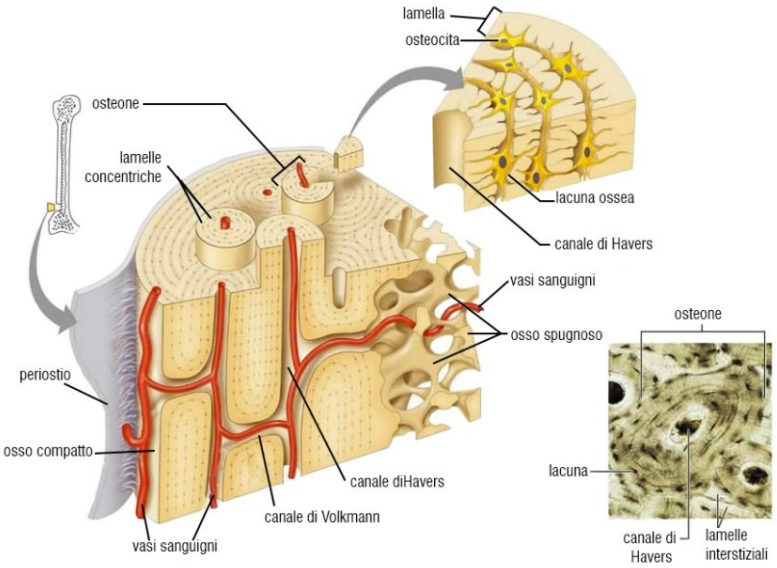

Figure 2: Cortical Bone Tissue Organization with focus in Osteon structure (II)

Analysing a section of cortical bone, it is possible to recognise:

- Periosteum: the outermost layer of fibrous nature is extensively vascularised and has the function of separating the bone tissue from other tissues and transporting nutrients.
- Osteogenic layer: in this part there is a marked cellular activity that allows the enlargement of the bone section and its modelling and is responsible for the healing process of a damaged bone.

Endosteum is the membrane lining the internal cavities that faces the medullary cavity.

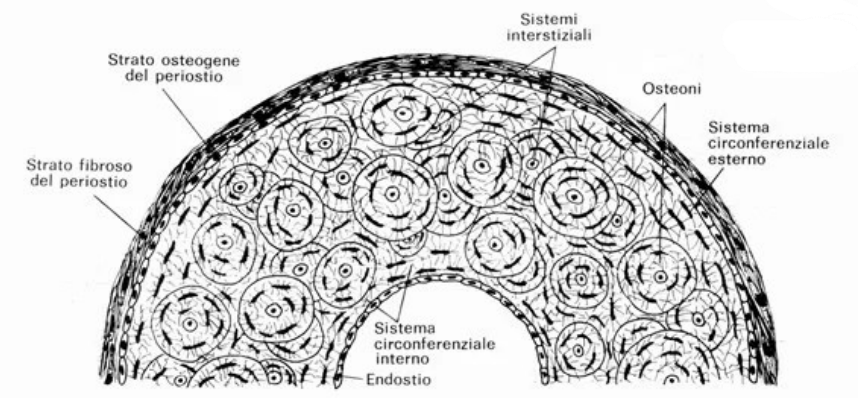

Figure 3: Cortical bone cross-section showing Endosteum and Periosteum (III)

Cellular Components

The cellular component of bone tissue is the interaction and coordination of four main cell types: bone lining cells, osteoblasts, osteocytes, and osteoclasts.

- Bone lining cells: due to their flattened shape, they form a cellular mat that separates the bone matrix from the extracellular environment, forming a layer that covers the bone surfaces. They form a barrier between the bone tissue and the surrounding environment by mediating molecular exchanges between the two compartments. The task of these cells is shape-shaping through erosion and deposition. The lining cells, together with the osteocytes, make up the permanent population of bone cells.

- Osteocytes: derive from the maturation of osteoblasts that, after losing the extracellular matrix, become trapped in specific areas called bone voids. Osteocytes are the most abundant cell type in bone tissue, as they can maintain the bone matrix and play a crucial role in mechano-transduction, the process by which mechanical forces are converted into biochemical signals that regulate bone remodelling. Their cytoplasmic extensions pass through Volkmann's channels that connect cells to each other and to blood capillaries, allowing the exchange of gases, nutrients and metabolic products. [3]
  - Osteoblasts: these are polyhedral monolayer-shaped cells 20-30 μm in size that juxtapose with each other to line small areas of matrix forming the mineralisation front. Osteoblasts are cells involved in bone formation through a process called osteogenesis, during which bone matrix is secreted that will later be mineralised. The deposition of organic substance occurs about 15 days before the mineralisation process, which lasts about 10 days. At the end of this process, some osteoblasts become trapped within the mineralised matrix and in this way transform into osteocytes. Osteoblasts originate through differentiation from mesenchymal stem cells and participate in the formation of the osteoid, a substrate of aligned collagen fibres to which hydroxyapatite crystals bind along preferential lines, giving the bone mechanical strength. Osteoblasts engage in the production of osteocalcin and osteonectin, proteins that support the deposition of calcified matrix. [4]
  - Osteoclasts: these are large multinucleated cells, 100 μm in size, responsible for bone resorption. Osteoclasts derive from haematopoietic stem cells and are part of the monocyte/macrophage lineage as they are crucial to the process of osteolysis for bone resorption. These cells can adhere to the surface of the bone to be resorbed, are

capable of secreting acids and proteolytic enzymes that dissolve the mineral component and degrade the organic matrix, forming the Howship gap along which osteoclasts are able to migrate to reach another region and continue the resorption process. This process is essential for bone remodelling and the maintenance of calcium homeostasis. [5, 6]

Bone Reshaping

Given its functional role, bone tissue undergoes continuous remodelling throughout life, which is essential for maintaining bone strength and repairing micro-damage.

Bone remodelling is a continuous biological process with two distinct main phases:

- Resorption: removal of old or damaged bone tissue
- Deposition (or apposition): formation of new bone tissue.

This process is of fundamental importance for maintaining skeletal health because through it, bone can be adapted to biomechanical needs, micro-damage can be repaired and calcium levels in the body can be regulated.

Bone remodelling occurs through the coordinated action of two main types of cells: osteoclasts, which are crucial in bone resorption, and osteoblasts, which are able to synthesise new matrix [7, 8].

The remodelling process is regulated by various factors, which may be:

- Protein:
    - Receptor Activator of Nuclear Factor κB Ligand (RANKL): is a protein expressed by osteoblasts and bone marrow stromal cells that can bind to its receptor RANK, located on the surface of osteoclasts and their progenitor cells. The interaction between RANKL and RANK is crucial for the differentiation, activation and survival of osteoclasts, initiating the process of bone resorption.
    - Osteoprotegerin (OPG): is a protein produced by osteoblasts that acts as a ‘decoy receptor’ for RANKL. Osteoprotegerin prevents RANKL from binding to its receptor, thus blocking osteoclast activation. The balance between RANKL and osteoprotegerin regulates osteoclastic activity and, consequently, bone remodelling.

- Hormones:
    - Parathormone (PTH): is a hormone produced by the parathyroid glands in response to low blood calcium levels, acting peripherally on the kidneys and bones. Parathormone stimulates the production of RANKL by osteoblasts by inhibiting the production of osteoprotegerin, promoting osteoclast activation and increased bone resorption to release calcium into the bloodstream.
    - Calcitonin: by binding to its receptors, calcitonin can inhibit osteoclast motility, thus inhibiting bone matrix degradation and calcium release. Unlike parathormone, calcitonin indirectly modulates the action of RANKL by reducing its effect.
- Calcitriol: the active form of vitamin D, increases RANKL expression in osteoblasts and stromal cells, facilitating osteoclast activation but not only: vitamin D is able to promote intestinal absorption of calcium, which is essential for bone mineralisation during the remodelling phase.
- Signals:
    - Macrophage Colony-Stimulating Factor (M-CSF): is a growth factor essential for the proliferation and survival of osteoclast progenitor cells. It is produced by stromal cells and osteoblasts and contributes to the formation of mature osteoclasts.
    - Prostaglandins: inflammatory molecules capable of stimulating the bone remodelling process. In particular, Prostaglandin E2 (PGE2), promotes RANKL production and osteoclast differentiation.
    - Growth factors (TGF-β and IGF): TGF-β (Transforming Growth Factor-beta) and IGF (Insulin-like Growth Factor) are involved in the regulation of bone remodelling. TGF-β is released during bone resorption and stimulates bone formation, while IGF promotes osteoblast proliferation and bone matrix synthesis
    - Cytokines: these are molecules involved in the regulation of bone remodelling. Some of them, such as IL-1 and TNF-α, can promote osteoclast activity and thus bone resorption.

For everything to work properly, there must be homeostasis, i.e. a balance between bone resorption and new bone formation, because when this balance is lacking, pathological conditions can occur too much bone resorption compared to formation can lead to osteoporosis, a condition in which bones become brittle and more susceptible to fractures.

The process of bone remodelling consists of five main phases: activation, resorption, reversal, formation and termination. The phases are interconnected and co-ordinated to ensure the structure and function of bone. [9, 10]

Activation

The first phase of remodelling begins with the detection of a signal that can be in the form of hormones, such as oestrogen or parathormone, or in the form of direct mechanical stress on the bone. The continuous stresses to which the skeleton is subjected are perceived by the osteocytes, which perform a transduction by translating the mechanical signal into a biological signal and initiating bone remodelling.

Parathormone (PTH) binds to its receptor located on pre-osteoblasts. Damage to the mineralised bone matrix causes localised apoptosis of osteocytes, reducing the local TGF concentration resulting in inhibition of osteoclast genesis.

In the bone microenvironment, PTH activates a receptor coupled to seven transmembrane G-proteins: the binding of PTH to its receptor activates protein kinase A, protein kinase C and the intracellular calcium signalling pathways, inducing a wave of transcriptional responses capable of modulating the secretion of molecules that recruit osteoclast precursors, inducing their differentiation and subsequent activation. At this point, bone resorption can begin.

Reabsorption

In response to PTH-induced bone remodelling, in vivo osteoblasts produce the chemokine MCP-1, a chemo-attractant for osteoclast precursors, which can enhance RANKL-induced osteoclast genesis.

MCP-1 is released by osteoblasts and can recruit pre-osteoclasts to the bone surface. Meanwhile, osteoblasts' expression of osteoprotegerin decreases while CSF-1 and RANKL production increases to promote proliferation of osteoclast precursors and differentiation of mature osteoclasts. Mature osteoclasts anchor themselves to their binding sites, creating a localised microenvironment called the sealed zone, which facilitates the degradation of mineralised bone matrix. In doing so, hydrogen ions are pumped into the sealed zone, which becomes acidic, promoting dissolution of the mineralised matrix and producing Howship resorption gaps. The remaining organic bone matrix is then degraded by a set of collagenolytic enzymes.

Inversion

Inversion cells incorporate and remove undigested demineralised collagen from the bone surface. Transition signals are generated that stop bone resorption and stimulate the bone formation process.

Following the bone resorption phase, osteoclasts undergo apoptosis, undergoing cell death or are simply removed from the site. Mononuclear cells derived from macrophages prepare the bone surface for the next formation phase by depositing a layer of protein matrix called osteoid.

Formation

Osteoblasts, cells responsible for building new bone, migrate into the cavity and begin depositing new bone matrix called osteoid. This matrix is subsequently mineralised to form mature, strong bone. Type I collagen is the primary organic component of bone. Non-collagen proteins, including proteoglycans, glycosylated proteins, SIBLING (small integrin-binding ligand) proteins, Gla-containing proteins (matrix Gla protein and osteocalcin) and lipids, make up the remaining organic material. For the bone to assume its final shape, hydroxyapatite is incorporated into this newly deposited osteoid.

Termination

When an equal amount of resorbed bone has been replaced, the remodelling cycle ends. After mineralisation, mature osteoblasts either undergo apoptosis or incorporate into the mineralised matrix and differentiate into osteocytes. The resting bone surface environment is re-established and maintained until the next remodelling phase begins. [11, 12]

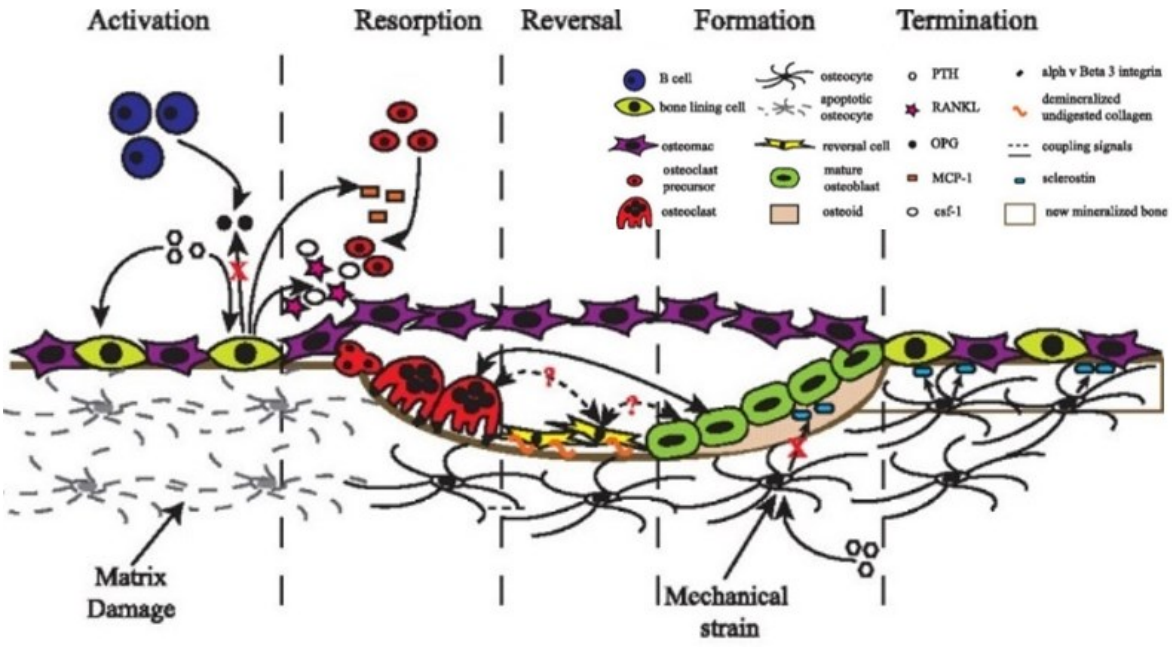

Figure 4: Stages of Bone Remodelling (IV)

The bone remodelling cycle can last several months and occurs in functional units called Basic Multicellular Units (BMUs), a coordinated group of cells that work in a synchronised manner to resorb and form new bone tissue.

Each BMU is composed of:

- Osteoclasts: BMUs begin with the activation of osteoclasts, which are responsible for the resorption of old bone. Osteoclasts excavate a cavity, called the Howship gap, in the bone tissue. This resorption occurs along a 'shear line' that moves through the bone.
- Osteoblasts: after resorption, osteoclasts are replaced by osteoblasts, which are responsible for the formation of new bone. Osteoblasts deposit osteoid, an organic matrix that subsequently mineralises to form new mature bone.
- Coordination and Signalling: BMUs operate under the control of a complex network of biochemical and mechanical signals. Local factors such as RANKL, M-CSF, and OPG, as well as systemic hormones such as parathormone and vitamin D, regulate the activity of cells within BMUs.

A single BMU can remain active for several months, completing a cycle of bone remodelling.

BMUs ensure that old and damaged bone is removed and replaced with new bone, allow bone to adapt to changes in mechanical loading, modifying bone density and structure according to functional needs, and contribute to the regulation of calcium and phosphate in the body, which are essential for many physiological functions in addition to bone health. [13, 14]

Osteoid is a non-mineralised organic matrix produced by osteoblasts during bone formation. Osteoid represents the first stage of new bone deposition and forms a structural network that will later be mineralised to form mature, rigid bone.

The osteoid consists mainly of:

- Type I collagen: accounts for about 90 per cent of the osteoid matrix. Collagen fibres give the matrix its structure and mechanical strength.
- Non-collagen proteins: about 10% of the matrix is made up of proteins such as osteocalcin, osteonectin, and alkaline phosphatase. These proteins play key roles in the regulation of mineralisation and in the interaction between bone cells and the matrix.
- Glycosaminoglycans and proteoglycans: these components contribute to the regulation of mineral deposition and the maintenance of matrix integrity.

The osteoid acts as a scaffold for the subsequent mineralisation process; in fact, following deposition, the osteoid sees the deposition of hydroxyapatite crystals between the collagen fibres, making the bone hard and resistant.

Mineralisation generally occurs within 10-12 days of osteoid formation, although this time may vary depending on the physiological or pathological condition of the individual. [15, 16]

Alterations in osteoid production, composition or mineralisation can lead to bone diseases such as:

- Osteomalacia: a condition characterised by defective osteoid mineralisation, leading to soft and weak bones.
- Osteogenesis imperfecta: a genetic disorder in which type I collagen synthesis is impaired, leading to defective osteogenesis and brittle bones.

Davy-Hart Model and Wolff's Law

Davy-Hart's Law is a central principle in bone regeneration according to which bone tissue can adapt dynamically to the mechanical stresses to which it is subjected. This behaviour is crucial in the process of bone regeneration.

Underlying this model is the behaviour of bone that responds to mechanical stress with functional remodelling:

- As load increases, osteoblasts are activated by increasing bone matrix deposition and improving its density.
- When the load stress decreases or disappears, the bone becomes more fragile and tends to lose mass. In this case, osteoclasts, cells that degrade the bone and reduce its density, come into play.

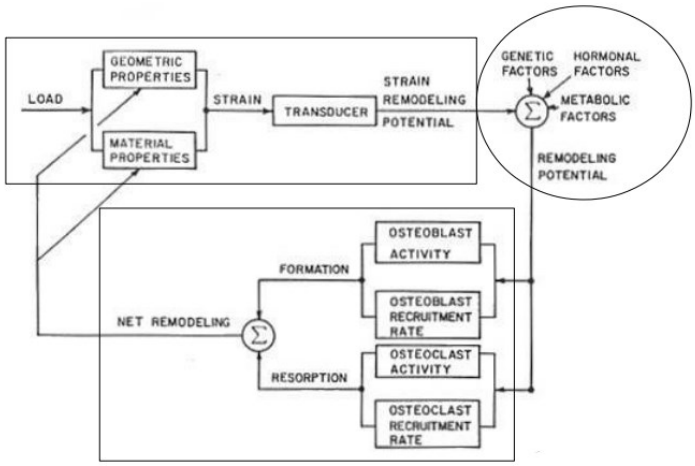

Figure 5: Davy-Hart Model (V)

The remodelling process is crucial for the adaptation of bone to mechanical loads. In this regard, it is worth quoting Wolff's law which states:

'The bones of the body remodel and adapt in response to the mechanical stresses to which they are subjected'.

This means that bone can organise itself and become stronger in areas where load or stress is applied, while it tends to become thinner and weaker in the absence of such stresses.

[17, 18, 19, 20]

Biomechanical Properties of Bone Tissue

As already mentioned, bone is a composite material that sees the presence of two main phases: the inorganic mineral phase composed of hydroxyapatite crystals that interpose themselves in the organic phase represented by collagen.

Molecules of this type come together to form first the fibrils and then the collagen fibres, which in turn interact to form the bone lamellae that differ in the orientation they acquire.

Bone is a viscoelastic material: it can deform under load and return to its original shape when the load is removed, but the extent of deformation also depends on the speed and duration of the load applied. The viscoelastic properties of bone are crucial to its ability to absorb energy and resist fracture under dynamic loading.

Bone strength is also influenced by factors such as bone mineral density, microarchitecture and bone matrix quality. Bone mineral density is a major determinant of bone strength and is commonly measured in clinical settings to assess fracture risk.

However, other factors such as trabecular connectivity, cortical thickness and the degree of mineralisation play important roles in determining bone strength and fracture resistance.

Cortical Bone

Cortical bone tissue is strongly anisotropic: the mechanical response along the direction of development of the osteons is better than in the other two perpendicular directions because there is greater stiffness as there is greater applied load. The behaviour can be said to be transversely isotropic, as along the other directions the stiffness is almost equal.

	Young Modulus
Proximal - Distal direction	E3 = 18.4 GPa
Radial direction	E2 = 6.91 GPa
Circumferential direction	E1 = 8.51 GPa

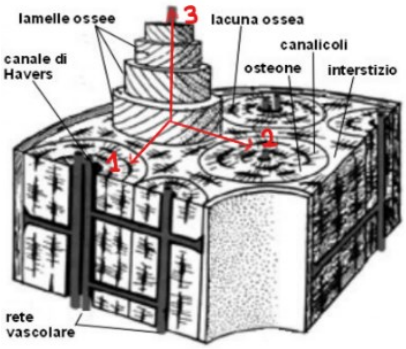

Table 1: Young's modulus of Tibia in different directions (I)

This behaviour is determined by the bone's own microstructure: the movement of the liquid phase allows the collagen fibres to stretch; this causes the lamellae to slide together allowing the osteons to move reciprocally.

Apatite crystals exhibit high strength and rigidity with an elastic modulus of approximately 165 GPa, unlike collagen which can be approximated at 2 GPa. The elastic modulus of cortical bone is 18 GPa, due to its microstructure.

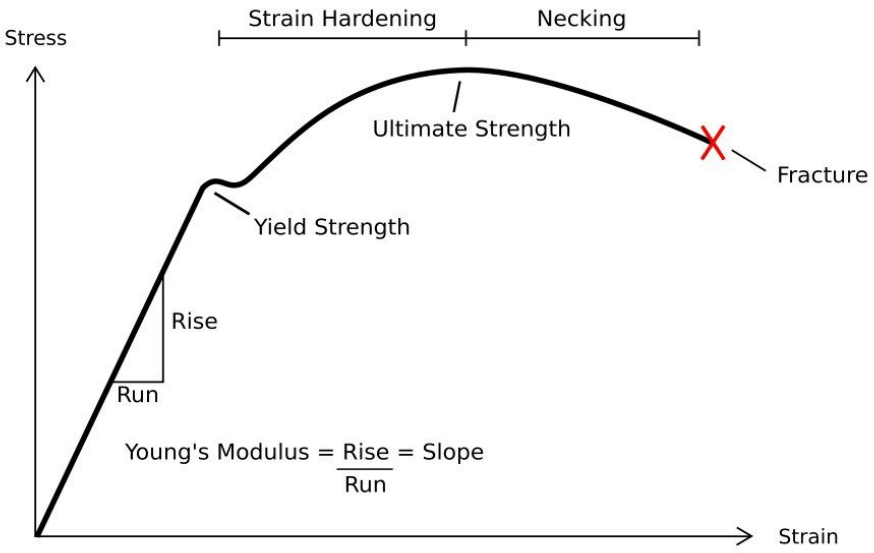

Figure 6: Stress-strain diagram for an elastic-plastic material (VI)

Collagen can increase the ductility of bone, improving its post-elastic behaviour, increasing shock absorption capacity and limiting the risk of complete fracture. It also promotes bone tenacity, i.e. the ability of bone to resist the propagation of fractures in its structure.

Mechanical behaviour is influenced by different factors:

- Orientation of the load: the mechanical behaviour is anisotropic as ductility is higher in the longitudinal direction.
- Age: advancing age induces a decrease in the amount of minerals in the body.
- Hydration: bone tissue is hydrated. As the fraction of liquid component decreases, the mechanical response worsens, showing an elastic-fragile pattern.

In general, cortical bone is characterised by high density and low porosity (5-10%), cortical bone is very resistant to both tensile and compressive forces; in fact, the Young's modulus in the longitudinal direction varies between 17 and 20 GPa implying that it is well able to deform elastically and return to its original shape once the load is removed.

Trabecular Bone

The mechanical behaviour of trabecular bone is de1 plenty like that of cortical bone: the constitutive model is anisotropic elastoplastic. What does change, however, is the mechanical response to tension, which is lower than to compression.

Trabecular bone is porous, and this characteristic influences its mechanical behaviour: as porosity increases in a region, mechanical properties decrease. Empirically, the Young's modulus in cortical bone correlates with the loading velocity and density:

$$E = 3790\dot{\varepsilon}^{0.06}\rho^{3}$$

$$\sigma^{-} = 68\dot{\varepsilon}^{0.06}\rho^{2}$$

With E (MPa) modulus of elasticity, σ^{-} (MPa) axial compressive strength, ρ (g/cm^3) structural density and ε (sec^{-1}) strain rate.

The structural configuration of trabecular bone tissue is strongly dependent on11 age: increasing age leads to a decrease in ultimate stress. The fracture of trabeculae also increases in relation to cyclic stress, leading to an increased risk of fractures.

Trabecular bone is characterised by high porosity (50-90%), which makes it much lighter, less tensile and compressive strength than1 cortical bone.

Young's modulus is also lower, ranging between 0.1 and 2 GPa, suggesting that it is better able to deform under load.

[21, 22, 23, 24]

	Cortical Bone	*Trabecular Bone*
Density	2kg/dm^3	0.15-1 kg/dm^3
Tensile Strength	130-220 MPa	2-12 MPa
Compressive Strength	70-150 MPa	1-5 MPa
Young Modulus	17-30 GPa	0.1-2 GPa

Table 2: Comparison between Cortical Bone and Trabecular Bone (I)

Chapter 2

Biomaterials

Since the earliest times, human beings have tried to use what was around them to improve their physical condition: from wood to emulate rudimentary prostheses to textile fibres to stitch up wounds to iron, in more recent times, to fix fractures.

One could refer to all these endeavours under the name of biomaterials, as they have characteristics such that they can be used in medicine for the construction of therapeutic and diagnostic devices.

In recent years, traditional biomaterials such as wood, metal and ceramics have increasingly been joined by all those techniques used in regenerative medicine, with the aim of replacing or repairing damaged tissues, supporting tissue regeneration and improving or replacing impaired biological functions, often from the patient's own cells.

Biomaterials Properties

When it comes to biomaterials, the watchword is biocompatibility: the material, whether implantable or not, must in no way induce adverse reactions in the body.

Since the 1970s, attempts have been made to define what it means to be biocompatible. In 1974, at the 6th Annual International Biomaterial Symposium, an elementary axiom was agreed upon:

"Biomaterial is a substance that is inert, both in relation to the organism and pharmacologically, designed to be implanted or incorporated into a living system".

In 1984, the first official definition was proposed in which drugs were excluded from the category:

"Biomaterial is any substance or combination of substances of synthetic or natural origin, other than a drug, that can be used for any period of time alone or as part of a system, that treats, augments or replaces any tissue organ or function of the body"

Up to the most current definition:

> *"Biomaterials are special materials that work in intimate contact with living tissue, minimising any adverse reactions or rejection by the organism."*

This definition highlights the importance of the interaction between the material and the biological tissue, a crucial aspect for the clinical success of biomaterials.

[25, 26]

Biocompatibility is one of the most important characteristics and is the ability of a biomaterial to integrate or interact with the surrounding tissue without inducing an unwanted immune response. This is crucial to ensure efficacy and safety during clinical application.

However, the design of biomaterials is not limited to the choice of biocompatible materials, but extends to the creation of three-dimensional structures, or scaffolds, capable of supporting cell growth and differentiation. Indeed, scaffolds not only provide mechanical support, but also create a microenvironment that promotes tissue regeneration by replicating the natural extracellular matrix. Their design requires a thorough understanding of the physic-chemical properties of the materials as well as the biological requirements of the tissue to be regenerated.

The evolution of biomaterials has been driven by advances in processing technology and the increasing understanding of biological mechanisms at the molecular level. From the first generation of inert materials, such as metals and polymers, we have moved on to active and resorbable biomaterials that can dynamically interact with the biological environment and, in some cases, degrade in a controlled manner a11 within the body. This evolution has opened new perspectives for regenerative medicine and the personalisation of therapies, enabling the development of solutions tailored to the specific needs of patients.

Obviously, it is not enough for a material to be only biocompatible, other properties are:

- Bio functionality: ability to effectively perform the function for which it was designed, such as replacing tissue or promoting tissue regeneration.
- Durability: ability to maintain its mechanical and functional properties over time, resisting degradation in complex biological environments.

- Processability: ability to be machined and moulded into appropriate shapes and sizes for clinical use.
- Bioactivity: ability to promote cell adhesion, proliferation, and differentiation.
- Immune response: ability of a biomaterial not to provoke an adverse immune response. This property is essential for its acceptance by the body.
- Bioinerzia: stability between the biological environment and the surface of the material, avoiding chemical and physical reactions.
- Biotolerance: ability of the material not to be eliminated by the body.
- Bioactivity: ability of the material to evoke reactions of all kinds, both favourable and unfavourable.

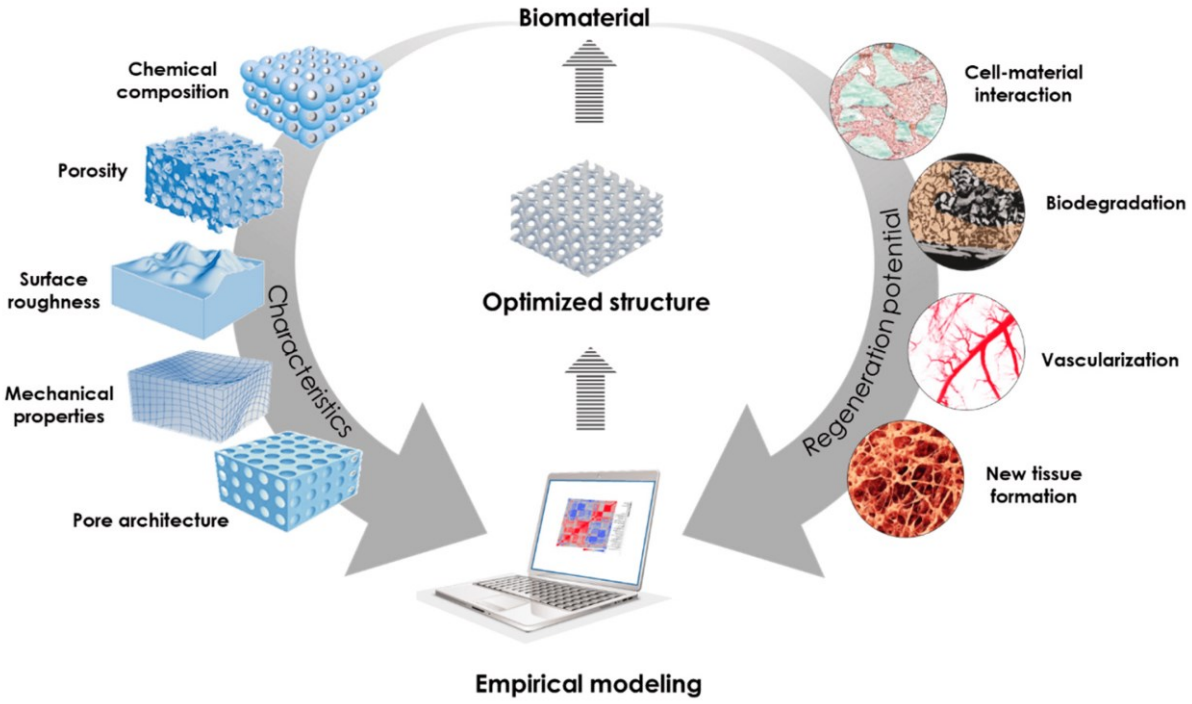

Figure 7: Connection between chemical-physical characteristics and regenerative potential (VII)

Biomaterials Classification

The classification of biomaterials is a crucial aspect for understanding characteristics, applications, and potential future developments.

Biomaterials can be classified according to their chemical composition into metals, ceramics, polymers, and composite materials.

- Metals: widely used due to their excellent mechanical properties such as hardness and fatigue strength. The chemical-physical properties of this class of materials play a key role in the choice of metals: as they can conduct heat and electricity, they are used for dental implants, joint replacements and in cardiovascular devices such as stents and valves. However, not all metals are biocompatible; in fact, one of the main problems is that they tend to corrode in a biological environment. The most used metals include stainless steels, cobalt-chromium alloys and titanium alloys, the latter exploiting titanium's ability to promote osseointegration.
- Ceramics: the fundamental characteristic of this category of materials is high hardness and compressive strength. Biomedical ceramics, such as hydroxyapatite and zirconia, are particularly prized for their biocompatibility and their ability to integrate with bone tissue, which is why this type of material is often used in orthopaedic and dental applications.
- Polymers: organic materials composed of long chains of repeated molecules. They are versatile and innovative as they possess a wide range of properties, from flexibility to biodegradability. Polymers can be natural, such as collagen and chitosan derived from biological sources, or synthetic, such as polyethylene and polymethyl methacrylate, designed to improve mechanical strength and degradative properties. Due to their flexibility and ability to be moulded into different shapes, polymers are used in a variety of applications, including tissue engineering scaffolds, vascular prostheses and drug delivery systems.
- Composite materials: made up of two or more separate materials which, when combined, exhibit superior properties compared to the individual components: greater strength and stiffness, corrosion resistance and greater lightness. The most common composites in biomedical engineering are composed of a polymer matrix reinforced with fibres, which, depending on the application, can be glass, carbon or Kevlar: this combination results in materials with high mechanical strength and good

biocompatibility, making them ideal for applications such as dental and orthopaedic implants.

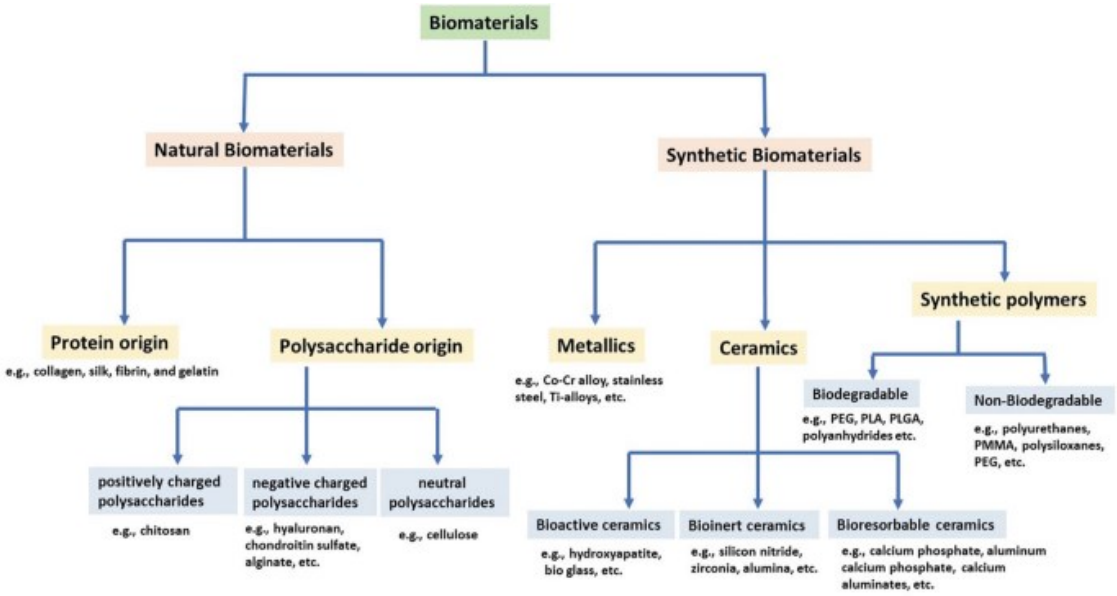

Figure 8: Biomaterial classification based on Chemical properties (VIII)

A further classification is based on how materials interact with biological tissues. This is done by dividing materials into three generations.

- First Generation Biomaterials or Bioinert: The first generation of biomaterials was designed to be bioinert, i.e. not to interact with the human body in any significant way. These materials, such as titanium alloys and stainless steels, were developed with the aim of avoiding adverse reactions from the immune system. Although these materials do not actively interact with tissues, the main issue is the lack of biological interaction and thus the risk of rejection, but despite this, their durability and resistance to wear make them still widely used today in prostheses and implants.
- Second Generation or Bioactive Biomaterials: designed to interact positively with biological tissues, stimulating a response to improve the functionality of the device or in the tissue itself. These materials, such as bioactive glasses and certain calcium phosphates, can stimulate a beneficial biological response, either by promoting the material's integration with the host tissue or by ensuring the complete bioresorbability, as in the case of polylactic and polyglycolic acids used for sutures and scaffolds for tissue regeneration. The limitation concerns biodegradation, which must be controlled to avoid inflammation and rejection.
- Third Generation or Bioabsorbable and Regenerative Biomaterials: also called dynamically interactive, they are designed not only to interact with tissues, but also to

promote tissue regeneration as they are capable of degrading gradually. These materials include bioabsorbable polymers and scaffolds for tissue engineering. The aim is to provide a temporary support that is gradually replaced by regenerated tissue, minimising the need for subsequent surgery to remove the implant.

Future prospects include the development of intelligent biomaterials, which can respond to biological or environmental stimuli, and the use of 3D printing technologies to create customised implants.

[30, 31, 32]

Ceramic Biomaterials

Ceramic materials are defined as inorganic, non-metallic solids obtained from processes involving hot temperatures. Depending on the electronegativity differences between the types of atoms that make up the lattice, the bonds may show a certain percentage of ionic and covalent character, as explained by the Pauling equation.

$$\%Ion\ Nature = 1 - e^{-\left(\frac{xA-xB}{2}\right)^2}$$

With xA and xB electronegativity of elements A and B. The crystal structure is determined by the extent of ionic or covalent bonding:

- In ionic ceramic solids, the atoms are arranged according to the size of the ions and the need to balance the charges to ensure electrical neutrality.
- In covalent ceramics solids, atoms arrange themselves according to directionality and bonding distance.

Ceramic Compound	Electronegativity Difference	%Ionic Bond	%Covalent Bond
ZrO_2	2.3	73	27
MgO	2.2	69	31
Al_2O_3	2.0	63	37
SiO_2	1.7	51	49
Si_3N_4	1.3	34.5	65.5
SiC	0.7	11	89

Table 3: Percentage of ionic and covalent bonding for certain ceramic compounds (IX)

Ceramics, obtained by processes involving the use of high temperatures, are known for their excellent mechanical, chemical and thermal properties such as resistance to compression, corrosion and heat.

Given their high stiffness, ceramic materials are often combined with polymer materials to exploit their high stiffness without, however, obtaining a brittle material: the ceramic fibres are able to strengthen the polymer matrix while the polymer slows down the propagation of fracture.

The fundamental properties of ceramics derive from their crystalline structure and the strong ionic or covalent bonds between atoms, which give them mechanical strength, high hardness, chemical resistance, and thermal and electrical insulation.

Despite all these advantages, ceramics are notoriously fragile materials, however, their ability to resist wear, hot temperatures and corrosion make them ideal for applications in extreme environments.

Ceramic solids have numerous defects within them that affect their structure and mechanical behaviour. Due to the chemical nature of the bond, the energy required for dislocations to flow is too high. Mechanical properties are most affected by the presence of:

- Grain Edges: ceramic materials are extremely sensitive to tensile stresses as these facilitate crack formation and propagation. Since there are few sliding systems in ionic solids, fracture occurs through crack formation at grain boundaries.
  This can be of two types:
  - Intergranular: the crack spreads along the grain boundaries due to impurities.
  - Trans granular: the crack spreads within the grain, changing direction of propagation at each grain edge.

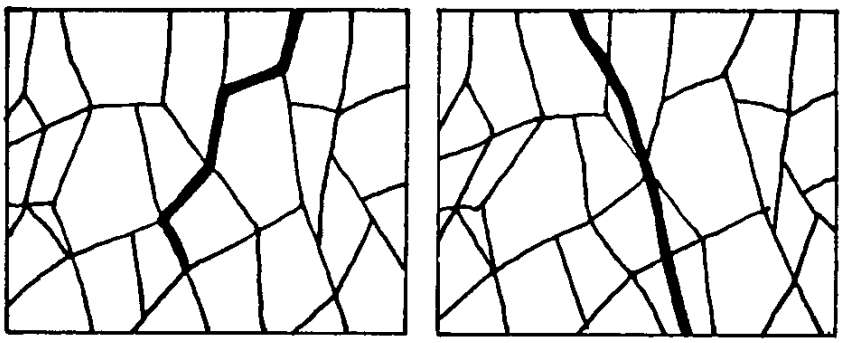

Figure 9: Intergranular and Transgranular cracks in Ceramic Biomaterials (IX)

- Porosity: pores are regions where stresses are concentrated; when a critical stress value is reached, cracks are formed and propagate. Through the sintering process, porosity can be eliminated by promoting coalescence through the formation of strong bonds.
- Grain Coarsening: slurring promotes uneven grain growth. This phenomenon makes the materials brittle.
    - If the grains are too small, it increases the likelihood of micro-cracks forming at the grain boundaries, promoting brittleness of the material.
    - If the grain is too large, the path of intergranular crack propagation is not very tortuous, requiring less energy for propagation and favouring the fragility of the material.

The mechanical behaviour of ceramic materials is typically elastic-fragile: the inherent brittleness of ceramic materials means that they do not give good mechanical responses in tensile tests, as the stress would propagate micro-fractures in the material. Excellent mechanical responses, however, are shown in compression, as the applied stresses will tend to pack the defects.

In covalent crystals, the bond is directional: a sufficiently high stress can cause a fracture due to the separation of electron pairs

In covalent crystals, equilibrium is disturbed by small shear stresses as the repulsion between ions of equal charge is sufficient to cause a brittle fracture. To measure the tensile stress necessary to break the bonds along a plane of the crystalline lattice, the theoretical cohesive strength is used.

[33, 34]

$$\sigma_L = \frac{Ea}{2\pi d} \approx \frac{E}{10}$$

Ceramic	σ_{th} = E / 10 (GPa)	E (GPa)	$\sigma_{f,tensile}$ (MPa)	$\sigma_{f,compressive}$ (MPa)
Alumina	127	380-400	260	4500
Zirconia	66	190-207	248	2500
Pyrolytic Carbon	9.5	28-30	207	500

Table 4: Theoretical cohesive strength for some ceramic compounds (IX)

Sphene

Calcium silicate-based ceramics are being explored as potential candidates for bone tissue engineering, as alternatives to traditional calcium phosphate ceramics and bioactive glasses. Sphene ceramics offer significantly higher chemical stability and enhanced biological performance due to the incorporation of Ca^{2+} ions into complex chains aligned along the a-axis, formed by corner-sharing [TiO_6] octahedra linked by isolated [SiO_4] tetrahedra.

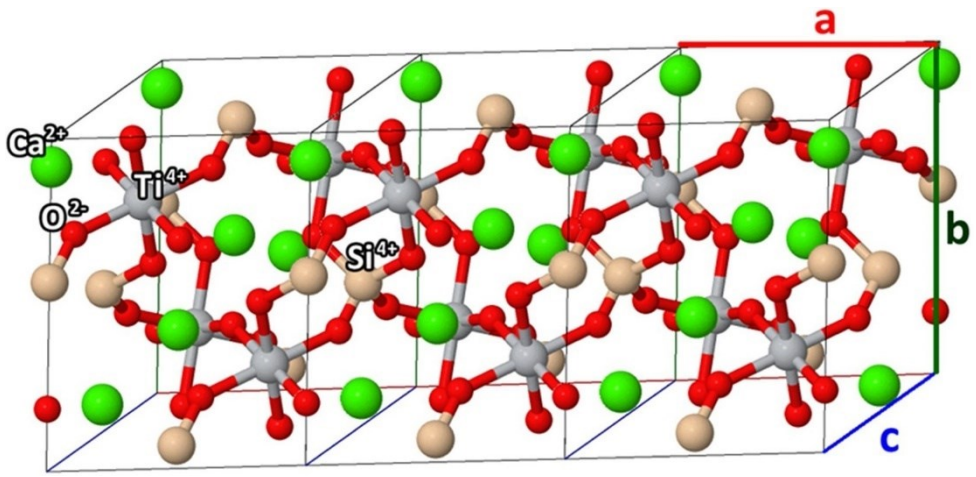

Figure 10: Sphene Structure (X)

Sphene can effectively promote bone formation around implants, enhancing osteointegration without inducing toxicity. A variety of fabrication methods have been employed to synthesize sphene ceramics, including sol-gel, coprecipitation, combustion, spray pyrolysis, freeze-drying, and hydrothermal processes.

However, achieving phase purity remains challenging, as sphene crystals are often accompanied by secondary phases such as cristobalite (SiO_2), perovskite ($CaTiO_3$), and wollastonite ($CaSiO_3$).

The similarity in thermal expansion coefficients between sphene and titanium has enabled the development of sphene coatings on Ti substrates using techniques such as plasma spraying, sol-gel, microarc oxidation combined with heat treatment, and airbrush spray coating.

These methods yield coatings with superior bonding strength and chemical stability compared to hydroxyapatite coatings. Furthermore, sphene biocoatings have been shown to enhance adhesion, proliferation, and differentiation of human osteoblast-like cells more effectively than coatings made of hydroxyapatite.

Silicone-based mixtures have already been successfully employed to produce sphene coatings. This study aims to expand the use of the polymer-derived ceramics approach for fabricating highly porous, phase-pure sphene reticulated scaffolds using Direct Ink Writing of a silicone-based paste. The printed sphene scaffolds exhibit varying porosities and pore sizes, featuring a hierarchical structure with fully interconnected porosity. The suitability of these scaffolds was confirmed through comprehensive in vitro and in vivo testing, which demonstrated promising biocompatibility and bioactivity, supporting their potential use in bone tissue applications.

[35, 36, 37, 38, 39, 40, 41, 42,43, 44, 45, 46, 47, 48]

Chapter 3

The ceramic process

The ceramic process encompasses the set of steps required to transform powders into a finished ceramic product. Although the steps in the production of biomaterials are the same as those used to make traditional ceramics, the focus is different: biomaterials that are biocompatible must be used.

Preparation of Powders

Powder preparation is the first step in the process: this is when the mechanical properties of the material to be obtained such as density, porosity and biocompatibility are defined.

Synthesis methods must be chosen according to the purpose of the finished product: in the field of biomaterials, the focus is on purity and controllability as these are essential characteristics to ensure proper osseointegration in vivo and avoid rejection.

Powder Characteristics	Requirements
Particle size	Thin (< 1μm)
Diameter distribution of the particle	Narrow or monodisperse
Particle shape	Spherical or equiaxial
State of agglomeration	Non-agglomerated or weakly agglomerated
Chemical composition	High purity
Phases present	Single phase

Table 5: Requirements for Powders (xi)

A key factor in the preparation of ceramic powders for biomaterials is the control of particle morphology and size distribution. These parameters directly influence the density and final microstructure of the sintered biomaterial. Particles must be homogenous to avoid aggregation and improve sintering, allowing for greater densification of the material:

- Narrow particle size distribution: it is preferable to have as narrow a particle size distribution as possible to improve densification during sintering.
- Particle morphology: spherical particles are generally preferred as they improve flow and compaction during moulding processes.

There are various types of techniques for preparing powders for ceramic biomaterials to produce particles of specific size and morphology, with high purity and uniformity.

Powder synthesis methods can be divided into mechanical and chemical:

- Mechanical methods: usually used for dust from naturally occurring materials
- Chemical methods: these are used to prepare powders from synthetic materials

In this section, the most common methods will be discussed in detail. [49, 50, 51]

Grinding and Crushing Mechanisms

Optimum particle size distribution can be achieved through crushing and grinding processes. These can be conducted in ball mills or planetary mills that use grinding bodies to reduce the particle size.

During these processes, the particles are deformed by mechanical impact or shear stresses and, if the stress is sufficient, breakage occurs. The mechanical energy released during grinding can induce physical changes, such as lattice rearrangements, but also chemical changes.

During grinding, it is crucial to avoid contamination due to the composition of the balls and to minimise the introduction of surface defects that could compromise the mechanical properties of the sintered material.

In ball milling, the crushing action occurs due to compression, friction and shearing mechanisms between the balls and the particles. Thanks to this process, it is possible to obtain particles with a diameter of 10 μm.

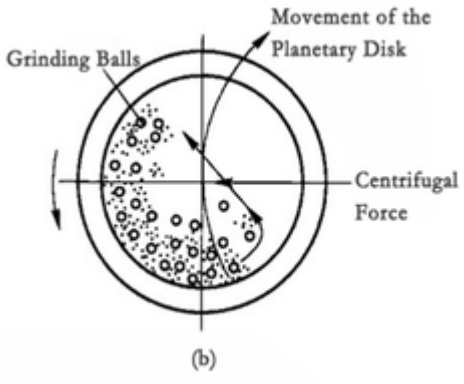

Figure 11: Horizontal section of a Grinding Jar (XI)

The major disadvantage of this process concerns the impossibility of further reducing the powder diameter below 1 μm: the grinding factor decreases along with the powder diameter.

Another problem concerns the wear of the balls, which could introduce impurities into the powder. This problem can be solved with the help of balls of the same material to be ground.

Jet mills are based on jets of gas (usually compressed air, but there are also systems that operate with the aid of inert gases) capable of transporting the powders to be ground at high speed, which collide with each other or against a barrier and shatter.

The spray drying technique is used to produce ceramic powders with controlled particle size from a liquid suspension containing solid particles.

The liquid is atomised by an atomiser into a high-temperature drying chamber, where the particles are rapidly dehydrated and collected as fine powders. This process is particularly useful for producing powders that are to be subsequently pressed or sintered, as it produces uniform, well-dispersed spherical particles, thus reducing defects in the finished material. There are different types of atomisers, such as pressure atomisers in which the solution is atomised by accelerating it thanks to a pressure difference, or ultrasonic atomisers that exploit the vibrations produced by a piezoelectric device.

[49, 52, 53]

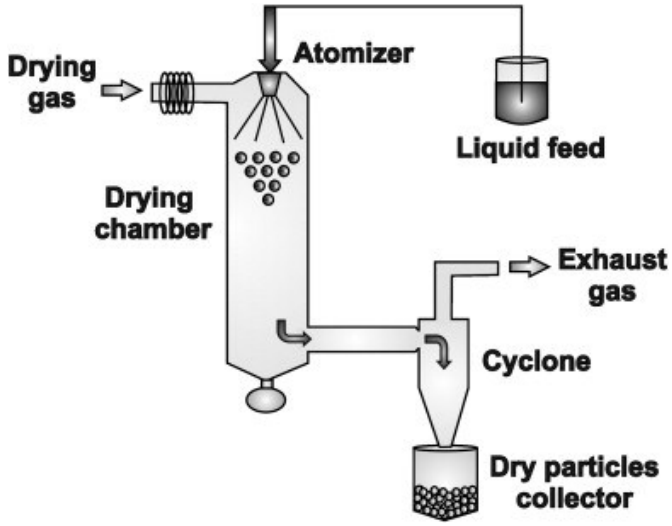

Figure 12: Spray-drying technique schematisation (XII)

Moulding

Forming processes are divided into traditional and non-traditional processes and are grouped into three sub-categories: dry pressing, plastic moulding and slip casting.

Dry pressing

The dry pressing process is one of the most established techniques in the processing of ceramic materials and is characterised by the application of pressure to compact the powders to obtain a green with reduced porosity that will be sintered.

Process variables are dictated by the pressure, which is between 50 and 300 MPa, material moisture and pressing speed.

Dry pressing is the most widely used technique to produce materials with simple geometries: the process allows high density to be achieved at the expense of less complex geometries. The critical points of dry pressing are due to:

- Particle size distribution: the particle size distribution of the ceramic powder directly influences the density of the green body and the final properties of the sintered product. A uniform distribution is crucial to avoid the formation of defects such as porosity and cracks during the sintering process.
- Pressure control: Too little pressure can lead to poor densification, while too much pressure can cause particles to fracture. Pressure control during pressing is therefore essential to ensure optimal density and prevent defects in the final component.

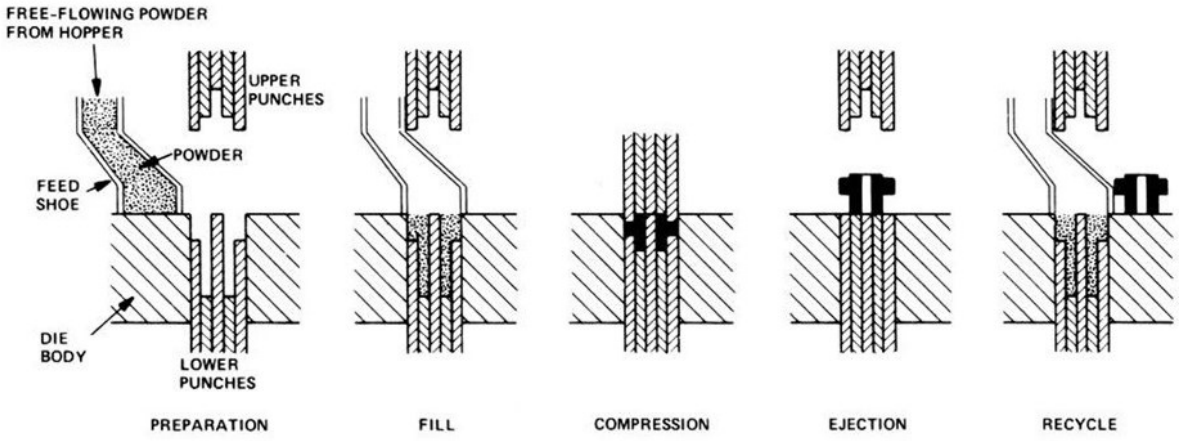

Figure 13: Uniaxial Pressing Schematisation (XIII)

Uniaxial pressing is the most common technique: the powder is placed in a rigid mould and compressed along an axis by a press. Uniaxial pressing is a simple and low-cost process, but geometries are limited.

Cold isostatic pressing is a more advanced technique than uniaxial pressing, as it applies pressure evenly to all sides of the component. The process is carried out by placing ceramic powder in a flexible container (usually of rubber or plastic) and then immersing it in a fluid (usually water or oil) inside an autoclave. Pressure is applied isotropically, allowing for a more homogenous densification of the material.

Through isostatic pressing, greater uniformity in density distribution can be achieved. It increases the ability to produce components with more complex geometries compared to uniaxial pressing. The main disadvantage is production costs.

Hot pressing combines mechanical compression with simultaneous sintering by applying pressure and heat at the same time. This method is particularly effective in reducing residual porosity and improving the mechanical properties of the bio-ceramic material. It is usually used for high-strength materials such as zirconium, which is used in the production of orthopaedic and dental implants.

[54, 55, 56, 57, 58]

Injection Moulding

Injection moulding is an advanced technique for the production of bio-ceramic components. This technique involves mixing ceramic powders with an organic binder to form a mixture (feedstock) to be injected into a mould at a controlled temperature. After cooling, the moulded component is removed from the mould and the binder is removed through a debinding process, which can be either thermal or chemical. Debinding is followed by the sintering phase, during which the component is heated to high temperatures to allow densification of the material.

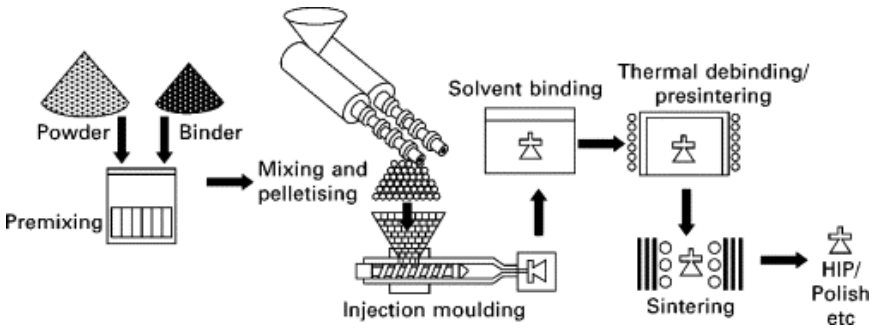

Figure 14: Injection Moulding Processing (XIV)

Injection moulding consists of three main stages: mixture preparation, moulding and sintering.

Feedstock formulation is a crucial step in the bio-ceramic injection moulding process: the organic binder is required to ensure the fluidity of the mix and its ability to fill the mould. The main problems relate to binder removal and shrinkage during the sintering phase:

- If the binder is not removed effectively, it can leave residues that adversely affect sintering, causing defects such as porosity and fractures.
- During sintering, the component undergoes volumetric shrinkage due to densification of the material. Shrinkage can be controlled using fillers so that the final object maintains the desired size and geometry.

[59, 60, 61, 62]

Stereolithography

Stereolithography is an additive manufacturing technique that uses the selective polymerisation of a photosensitive resin containing bio-ceramic powders, induced by a laser beam. This method makes it possible to obtain complex three-dimensional structures with high precision and detailed porosity control.

This process is particularly advantageous for the production of scaffolds used in bone regeneration applications, as the porosity can be modulated to promote cell growth and integration with the surrounding bone tissue. Stereolithography, adapted to the production of bio-ceramic materials, is a promising technology for the manufacture of highly customised medical devices. The process is based on the use of photopolymer resins loaded with ceramic particles, which are solidified layer by layer using an ultraviolet light beam. Once printing is complete, the part undergoes a sintering process that removes the polymer resin, leaving a dense ceramic structure.

The stereolithography process to produce bio-ceramics can be divided into three main steps:

1. Preparation of the ceramic resin: a photopolymer resin is mixed with biocompatible ceramic particles. The concentration of ceramic particles directly influences the mechanical and biological properties of the final part.
2. Stereolithographic printing: the three-dimensional model, created using CAD software, is divided into thin layers. Each layer is polymerised through a UV light

beam that solidifies the ceramic-filled resin. This process makes it possible to obtain complex and detailed structures with a resolution of up to 10µm.

3. Post-processing and sintering: after printing, the part is cleaned of the non-solidified resin. It is then subjected to sintering, a thermal process that removes the polymer matrix and consolidates the ceramic particles, producing a final high-density bio-ceramic object.

Optimisation of the stereolithography process mainly concerns the uniform distribution and size of the ceramic particles within the photopolymer resin:

- The homogenous distribution of ceramic particles is essential to ensure that the final material maintains consistent mechanical and biological properties across the entire surface.
- The choice of ceramic particle size affects the resolution of the printing process and the final mechanical properties of the part. Smaller particles tend to offer better resolution and higher final density but may increase the viscosity of the resin and make the printing process more complex.

One of the main advantages of stereolithography in the production of bio-ceramics is the possibility of creating complex, customised structures with high resolution and dimensional accuracy. This makes stereolithography particularly suitable to produce dental and orthopaedic implants, where a high degree of detail and anatomical fit is required.

In addition, the ability to control the porosity of the structures allows scaffolds to be designed with an optimised internal structure for tissue regeneration. This feature is essential to promote bone growth and vascularisation within the implants.

Despite its numerous advantages, stereolithography has some limitations in the processing of bio-ceramics. One of the main problems is the fragility of ceramic materials after the sintering process, which can lead to cracks or deformations, especially if temperature conditions are not carefully controlled. Furthermore, the mechanical properties of bio-ceramics produced by SLA are often inferior to those of materials produced by traditional techniques such as pressing or casting.

Another limitation concerns the settling of ceramic particles in the resin during printing, which can cause uneven particle distribution and affect the mechanical and biological properties of the final part.

[63, 64, 65, 66]

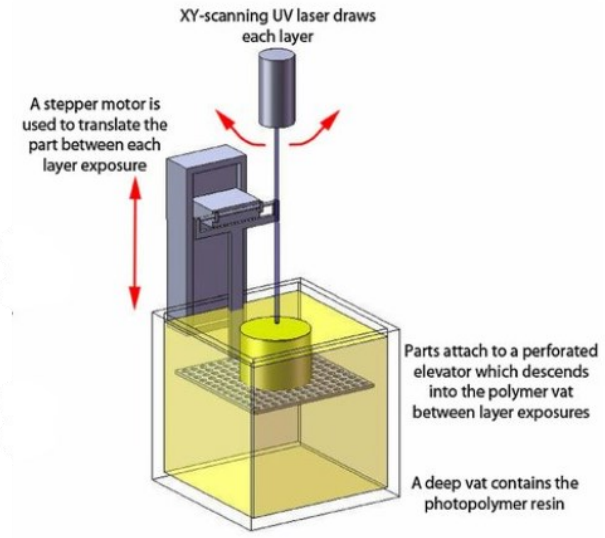

Figure 15: Stereolithography Additive Manufacturing System (XV)

Lost-Wax Casting

Lost-wax casting is a traditional method used for the manufacture of complex, precision bio-ceramic components. The process begins with the creation of a wax model of the desired component. This model is covered with a ceramic shell which, once solidified, is heated to melt and remove the wax. Finally, the shell is used as a mould for casting the bio-ceramic material. This method is particularly suitable for the production of dental implants and complex-shaped prostheses, where geometric precision is of paramount importance.

[67, 68]

Techniques	Advantages	Disadvantage
Dry-Pressing	High density and simply process	No complex geometries
Injection Moulding	Complex Geometries and mass production	Needs debinding
Stereolithography	High precision and high porosity control	High Cost
Lost-Wax-Casting	Complex geometries	Long processing times

Table 6: Processes Advantages and Disadvantages

Direct Ink Writing

Direct Ink Writing (DIW) is an Additive Manufacturing technology that enables the three-dimensional printing of ceramic, polymeric and composite materials through the controlled extrusion of a highly viscous ink. This technique is particularly promising for the production of complex structures used in advanced medical applications, such as scaffolds for bone regeneration, customised dental implants and prostheses.

In the field of bio-ceramics, DIW allows materials to be printed using inks specifically formulated to achieve good stability during the extrusion process and robust post-process sintering.

DIW is based on the controlled extrusion of a ceramic ink through a nozzle that deposits the material in overlapping layers following a predefined trajectory, which is managed through CAD models. The ink must have optimised rheological properties: high viscosity to retain its shape after extrusion and low surface tension to avoid the formation of surface defects.

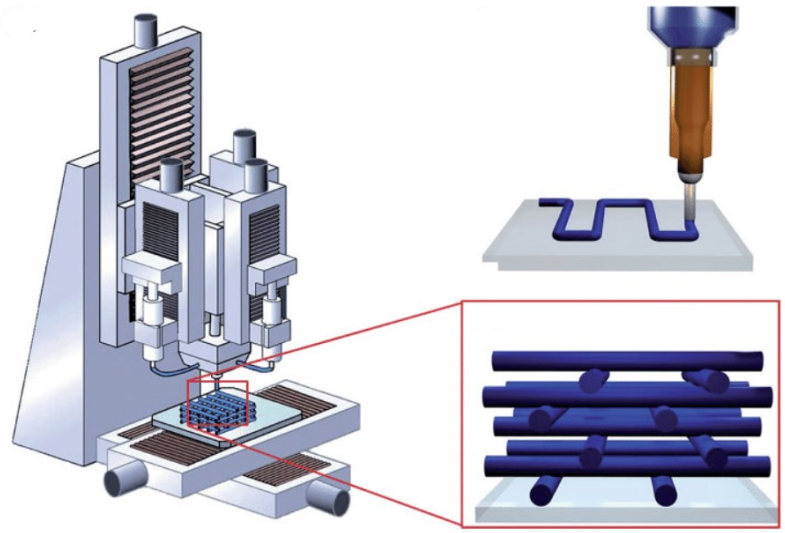

Figure 16: Direct Ink Writing Printing Method (XVI)

The ink used for DIW of bio-ceramics generally consists of:

- Bio-ceramic powder: which forms the basis of the material; • Solvents and additives: used to adjust the viscosity and rheology of the ink, typically water or organic solvents.
- Binders and stabilisers: to maintain system stability during the printing process and prevent sedimentation of ceramic powders.

Rheology is a crucial aspect in the DIW process. The ink must have a pseudo-plastic behaviour, in which the viscosity decreases under the action of a stress (during extrusion) and increases again once the stress is removed, allowing the material to retain its deposited shape. The stability of the ink is crucial to avoid phase separation during printing.

The main steps of the DIW process include:

- Digital design: the CAD model of the desired component is designed and converted into extrusion paths (g-code).
- Ink preparation: ceramic powders are mixed with solvents and additives until an ink with the desired rheological properties is obtained.
- Printing: Ink is extruded through a nozzle, following programmed paths to build the component layer by layer.
- Drying and consolidation: once printed, the component is dried to remove excess solvent.
- Sintering: the component is subsequently sintered high temperatures to achieve final densification and improve mechanical properties.

One of the main applications of DIW for bio-ceramics is the production of scaffolds for bone regeneration. Thanks to its ability to produce highly porous structures with complex geometries, DIW enables the manufacture of scaffolds that mimic the natural structure of bone, promoting cell growth and integration with biological tissue.

Bio-ceramic scaffolds, such as hydroxyapatite and calcium phosphates, are known for their bioactivity, stimulating the deposition of new bone tissue. DIW also makes it possible to control porosity and pore distribution, key parameters for optimising nutrient diffusion and bone integration.

DIW technology is ideal for the manufacture of customised implants for patients, such as dental prostheses or orthopaedic implant parts. Using 3D scans of the patient, highly customised bio-ceramic components can be designed and printed, with geometries that perfectly match the patient's anatomy. This approach reduces the risk of rejection and improves device integration.

[69, 70, 71, 72, 73, 74, 75]

Sintering

Sintering is the process that transforms powders whose particles are weakly cohesive into a dense, stable and resistant solid.

From a thermodynamic point of view, the process is favoured because the decrease in total surface area, and the exchange between solid-gas interfaces and solid-solid interfaces, favour the release of surface energy, favouring the packing of crystalline structures, removing interstitial porosity, and changing the shape of the initial particles.

The process takes place at temperatures around 2/3 of the melting temperatures.

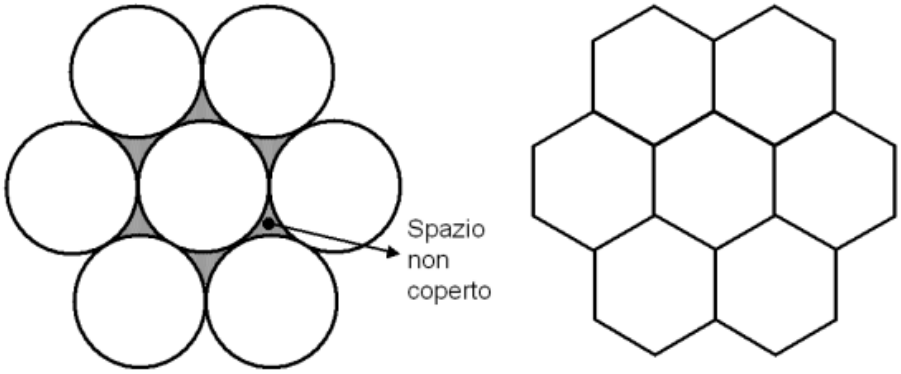

Figure 17: How sintering works for covering 3D space (XI)

There are three mechanisms, and they differ in the methodology of particle deformation:

- Sintering in the solid state: deformation occurs by diffusion.
- Sintering in the presence of a liquid phase: the liquid, present in a minimum quantity, has the task of reshaping the solid particles.
- Sintering by viscous flow: the liquid phase is generated from the transformation of particles that subsequently solidify.

Sintering in the solid state is the process that best allows the solid to be resistant at high temperatures due to the diffusive processes; in the other mechanisms, due to the liquid phase, the process takes place at lower temperatures but the glassy phase that is formed softens because of a further heating process, causing deformities.

Sintering is divided into three stages:

- Initial stage: junction necks are formed between the particles, which increase the density very little compared to green, from 60 to 65%.

- Intermediate Stage: the particles approach each other by interpenetrating. It is here that the change in geometry begins, moving from a spherical to a polyhedral shape that better allows packing. The final density changes from 65% to 90%.
- Final stage: the isolated pores are removed very slowly. It is during this stage that the last 10 per cent compaction is acquired.

Solid-state sintering

Sintering in the solid state occurs due to the difference in concentration: matter tends to migrate from convexity to concavity due to the different vapour pressure.

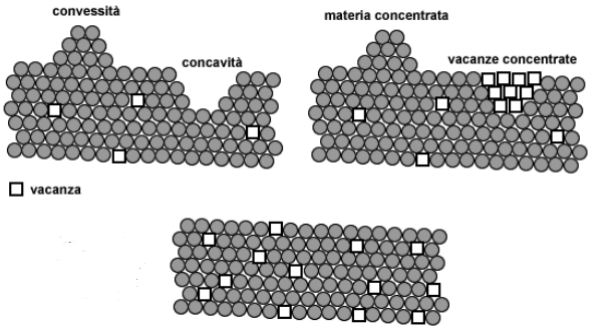

Figure 18: Vacancy-concentration transportation in Bioceramic Materials (XI)

The opposing motion between atoms and vacancies favours the formation of a neck that allows densification only if the transport of matter from the grain boundary to the neck occurs via grain boundary or via crystal lattice, or if the transport of dislocations to the neck occurs via crystal lattice.

In this way, the deformation of the particles makes it easier for the particles to close the gaps between them.

$$\frac{\Delta V}{V_0} = K' \cdot \frac{t^n}{r^m}$$

Where:

K': parameter dictated by the transport mechanism.

V0: initial volume.

r: particle radius.

t: sintering time.

The enlargement of the neck due to the transport mechanisms causes the change in shape from spheres to polyhedral: the monocrystalline particles bind together to form grains. At the point of intersection between three grains there are channels in which the atom/vacancy exchange continues. The process continues until the cylinders turn into isolated pores due to the reduction in diameter that accelerates the exchange of matter.

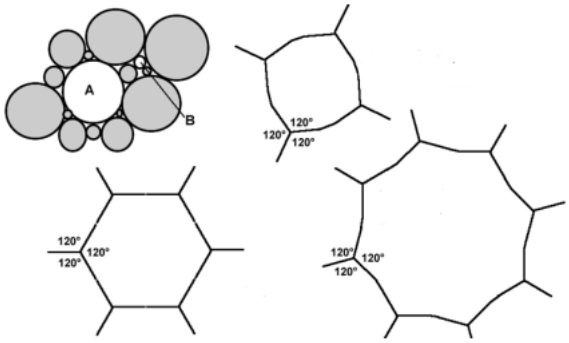

Figure 19: Grain stabilization by number of sides (XI)

Atom/vacancy motions continue as pores between many grains are difficult to encompass unlike those surrounded by four grains at most. The phenomenon of pore elimination is also complicated by grain growth: when three grains meet, the three interfaces are isoenergetic at 120° angles; this is the case for six-sided grains.

Grains with less than six sides tend to be encompassed by those with six or more sides that grow: thus, the pores between the small edges, once they are encompassed, are impossible to eliminate.

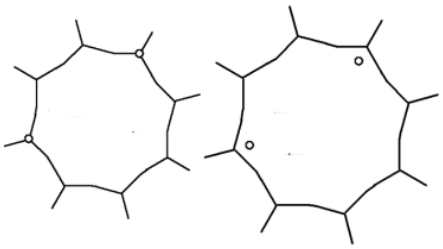

Figure 20: Stabilisation of Porosity by grain growth (XI)

The use of additives, such as magnesium oxide and titania, can promote densification by stabilising the edges.

Sintering in the presence of liquid phase

Ceramic materials characterised by covalent bonding are not sinterable in the solid phase. In this case, the presence of a liquid phase is useful, which allows agglomeration by facilitating the transport of matter: this occurs due to the diffusive/precipitative mechanism.

The limitation of the liquid phase is elevated temperatures: the softening of the glassy phase that occurs from the solidification of the liquid phase conditions the resistance to creep phenomena.

Sintering by viscous flow

The viscous flow sintering mechanism occurs due to a fraction of material melting around temperatures of 1100°C to 1200°C, incorporating mullite and silica and melting quartz that will solidify into glass.

Sintering by viscous flow, in its initial phase, is explained by Frenkel's law:

$$\frac{\Delta V}{V_0} = C\frac{\gamma t}{\eta r}$$

Where:

γ: surface tension.

η: viscosity.

r: particle radius.

t: sintering time.

C: constant.

[49, 76, 77]

Chapter 4

Materials and Methods

The purpose of this chapter is to illustrate the experimental section of this thesis, which was carried out within the laboratories of the Department of Industrial Engineering (DII) of the University of Padua.

It is therefore necessary to present the materials, the instrumentation used and the experimental procedure for the fabrication of sphene ($CaTiSiO_5$) scaffolds supported by pre-ceramic polymer emulsions.

Emulsion-supported materials have been shown to have enormous potential for 3D Direct Ink Writing as they exhibit pseudoplastic behaviour that is useful for easy extrusion: the ink exhibits low viscosity at the nozzle exit, which increases allowing the ink to retain its shape once deposited.

Once extruded, the scaffolds were heat-treated at 1300°C and characterised.

Materials

In this work, two distinct types of scaffolds were obtained from inks based on two different combinations of active fillers: TiO_2 and calcium nitrate tetrahydrate and TiO_2 and calcite ($CaCO_3$). The materials used are now presented.

- SILRES® H44 (Wacker-Chemie, Munich, Germany): a pre-ceramic polymer based on silicone resin in the form of a nano powder consisting of methyl-phenyl polysiloxanes. (1)
- Titanium Dioxide Nano Powder, Anatase, Inframat® (Advanced Materials, New York, USA): filler in nano powder form, useful for limiting volumetric shrinkage of the pre-ceramic scaffold during pyrolysis ~ 40 μm. (2)
- $Ca(NO_3)_2$-$4H_2O$ (VWR Chemicals, New York, USA): calcium nitrate tetrahydrate was used as a source of calcium oxide. (3)
- FunToDo (FunToDo, Alkmaar, The Netherlands): a transparent photosensitive resin capable of rendering green scaffold flexible following extrusion. (4)

- $CaCO_3$ (Industrie Bitossi, Vinci, Italy): white micro-sized powders insoluble in water ~10 µm. (5)
- N-hexane (Sigma-Aldrich®, St. Louis, Missouri, USA): widely used solvent for the preparation of stable suspensions as it acts as a volatile organic phase that evaporates rapidly after deposition of the material. (6)

Property	Value
Ash content (after pyrolysis at 1000 °C)	approx. 77 wt. %
Bulk density	450 kg/m³
Carbon content (cured resin)	approx. 46 wt. %
Colour	White Dark
Softening point	45 - 60 °C

Table 7: Silres ® H44 Properties

Instrumentation

For the sake of completeness, the instrumentation used, present in the laboratories of the Department of Industrial Engineering at the University of Padua, is reported.

Mechanical stirrer rod

Figure 21: AM 20-D (ARGOlab, Modena, Italy) (XVII)

The AM 20-D (ARGOlab, Modena, Italy), a propeller-driven model designed to mix and agitate liquids of different viscosities in volumes of up to 20 litres, was used as agitator. The stirring speed varied from 50 to 2200 rpm: for the sphene formulation, the speed varied from 600 rpm during the addition of the aqueous phase to the oily phase to 2200 rpm after the addition of n-hexane in order to obtain emulsion. (7)

Mixer

The Thinky ARM-310 (Thinky Corporation, Tokyo, Japan) is a vacuum-free planetary mixer designed to mix and disperse materials quickly and efficiently, using a planetary motion that enables uniform mixing without the use of blades.

The Thinky can be used for mixing and degassing and is capable of operating at a speed of 2000 rpm.

In this work, the use of the Thinky was mostly limited to degassing operations in order to remove air bubbles from the syringe and proceed with ink extrusion. (8)

Figure 22: Thinky ARM-310 (Thinky Corporation, Tokyo, Japan) (XVIII)

Printer

The Delta WASP 2040 PRO (WASP, Massa Lombarda, Italy) is a 3D printer suitable for rapid prototyping and the production of high-quality objects made from various materials.

Figure 23: Delta WASP 2040 PRO (WASP, Massa Lombarda, Italia) (XIX)

The printer has an auto-calibration system that adjusts the print bed automatically and a ground print bed that improves the adhesion of the material to the bed, reducing the risk of warping and defects.

The samples are printed by deposition of the extruded ink through a 0.84 mm nozzle that can move at a speed of 500 mm/s. (9)

UV-Chamber

Polymerisation was made possible through the use of a UV chamber. In this work, the Original Prusa CW1 (Prusa Research, Prague, Czech Republic), a combination unit for post-print polymerisation (curing) of 3D resins, was used.

Polymerisation takes place thanks to the presence of four UV lamps, arranged in such a way as to ensure uniform polymerisation of the 3D resin prints: the UV lamps emit light at a wavelength of 405 nm, which is ideal for solidifying the photosensitive resin, ensuring that the entire object is treated homogeneously during the post-curing process. (10)

Figure 24: Original Prusa CW1 (Prusa Research, Praga, Repubblica Ceca) (XX)

Stereomicroscope

The stereomicroscope is an optical instrument designed to observe three-dimensional objects at low magnification.

Figure 25: Zeiss Stemi 2000-C (Zeiss, Thornwood, New York, USA) (XXI)

The stereomicroscope provides a three-dimensional view of the object, thanks to two separate optical paths that offer two slightly different images for each eye. The model used in this thesis is the Zeiss Stemi 2000-C (Zeiss, Thornwood, New York, USA), which can offer variable magnification from 6x to 50x, with the possibility of further extending the range through additional lenses. (11)

Electronic Microscope

The Quanta 200 SEM (Thermo Fisher Scientific, Eindhoven, Netherlands) is a scanning electron microscope used for high-resolution surface analysis of samples, offering detailed images. The operating principle of an electron microscope is based on the use of an electron beam instead of light to obtain high-resolution images of very small samples. The electron microscope uses a tungsten filament as an electron source, which is able to generate electrons through thermal excitation. The electrons are accelerated by an electric field to obtain the energy needed to penetrate materials and achieve high resolution.

The kinetic energy of the electrons is focused into a thin beam through the use of electromagnetic lenses: current coils that generate magnetic fields to direct and focus the electron beam.

The principle of operation is as follows: the sample is placed inside the microscope chamber and invested by an electron beam which, on interacting with the sample surface, produces signal electrons. These electrons emitted by the sample are collected by detectors and converted into images visible on a monitor in real time. (12)

Figure 26: Quanta 200 SEM (Thermo Fisher Scientific, Eindhoven, Paesi Bassi) (XXII)

X-ray Diffractometer

X-ray diffraction (XRD) uses the interaction between X-rays and atoms in a crystal to determine the internal atomic arrangement of the structure.

The X-ray generator generally consists of a tungsten filament (cathode) which, when energized at low voltage, is able to heat up, emitting electrons due to the thermionic effect. The electrons are accelerated by the electric field due to the potential difference between anode and cathode, striking a metal plate (anode) and generating X-rays.

When an X-ray beam strikes a crystalline solid, the rays are diffracted according to the Bragg's law, which describes the necessary condition for constructive diffraction to occur:

$$n\lambda = 2dsin(\theta)$$

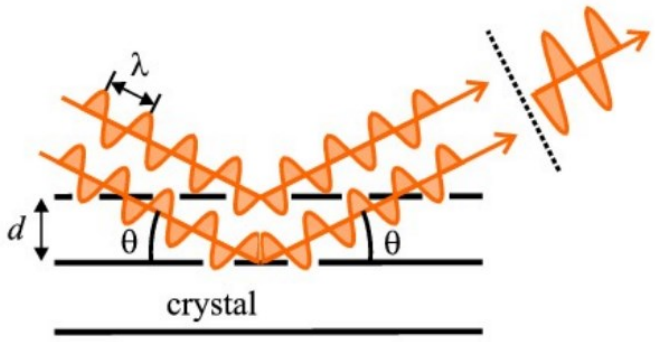

Figure 27: XRD operating principle (IX)

Where:

n is the diffraction order,

λ is the wavelength of X-rays,

d is the distance between the crystal planes (lattice spacing),

θ is the angle of incidence of X-rays.

[34]

To perform the analysis, the powders were ground and distributed on a metal sample holder, trying to obtain a uniform surface. The Bruker AXS D8 Advance (Bruker, Karlsruhe, Germany), an X-ray diffractometer designed for material analysis, was used as the instrument. During the measurement, the sample holder remains stationary, while the X-ray tube and receiver move together, increasing the angle of rotation by Δθ relative to the horizontal. The instrument was set with a voltage of 40

44kV and a current of 40 mA. Measurements were taken over an angular range 2θ between 15° and 70°, with an increment of 0.05° per second.

Phase identification was subsequently performed with the Match! (Crystal Impact GbR, Bonn, Germany). (13)(14)

Figure 28: Bruker AXS D8 Advance (Bruker, Karlsruhe, Germania) (xxiii)

Pycnometer

In order to determine the density of the material obtained, i t was necessary to use the Ultrapyc 3000 pycnometer (Anton Paar, Graz, Austria). This instrument has two calibrated cells: in the first stage of measurement, the reference cell is filled with helium at known pressure and volume, while the sample cell is depressurised. Subsequently, the helium is brought into the measuring cell, causing a change in pressure. The pycnometer then calculates the sample volume based on the pressure difference between the two cells. The device takes eight measurements and provides an average value. After entering the mass of the sample, the pycnometer calculates and reports the corresponding density. (15)

Figure 29: Picnometro Ultrapyc 3000 (Anton Paar, Graz, Austria) (XXIV)

Mechanical Press

The mechanical press used for the mechanical characterisation of the material is the Quasar 25 (Galdabini, Varese, Italy). The sample is placed on a steel plate, covered by parafilm, and a second plate moves in a vertical direction with an adjustable speed. The load cell instantly measures the resistant force offered by the sample and the corresponding programme on the PC graphically reports it as a function of the time coordinate. (16)

Figure 30: Quasar 25 (Galdabini, Varese, Italia) (XXV)

Furnace

A TERSID© elite BRF muffle furnace (Sesto San Giovanni, Milan, Italy), capable of reaching and maintaining high temperatures, was used for the necessary heat treatments.

Figure 31: TERSID Elite BRF ((Sesto San Giovanni, Milan, Italy) (XXVI)

The oven is equipped with a Eurotherm 2416 CG PID control system with a double display, programmable with 8 free format segments. Each segment can be programmed by setting the heating speed, as an increasing or decreasing temperature ramp, maintaining a constant temperature or the end of the programme. The heating system consists of silicon carbide heating elements, placed at the sides of the central chamber, which can bring the oven up to 1600°C. (17)

Manufacturing Methods

The aim of this work was to obtain sphene scaffolds from inks made from an emulsion composed of a preceramic polymer combined with fillers. Emulsion ink is based on the preparation of two distinct phases: an oily phase and an aqueous phase.

Calcium Nitrate Tetrahydrate

The oil phase is obtained by dissolving H44 powder in 4g of transparent photosensitive FunToDo resin. The mixture is allowed to rest overnight away from light sources to allow the powder to disperse within the polymer.

The following morning, 2g of Span80 (Sorbitan Monooleate, Tokyo Chemical Industry Co., Tokyo, Japan) must be added to the oil phase. This substance acts as a surfactant allowing the two phases to mix. Following the addition of Span80, everything is placed under the shaker at a speed of approximately 400-600 rpm.

The aqueous phase, on the other hand, involves the use of water in which the fillers are dissolved: calcium nitrate tetrahydrate salts and titanium oxide (TiO_2).

Using a pipette, the aqueous phase is slowly placed inside the oily phase under a stirrer working at a speed of 600 rpm.

After 10 minutes, it is time to add 1.5ml of n-Hexane, increasing the speed of the mixer to 2200 rpm so that the emulsion takes place.

Two different types of composition were tested: In the first, 2.91g H44 was used.

Fase Oleosa	*Fase Acquosa*
2.91g H44	2.03g TiO_2
4g FunToDo	5.98g $Ca(NO_3)_2 \cdot 4H_2O$
2g Span80	10g H_2O

Table 8: Calcium Nitrate Tetrahydrate 1st Ink formulation (XXVII)

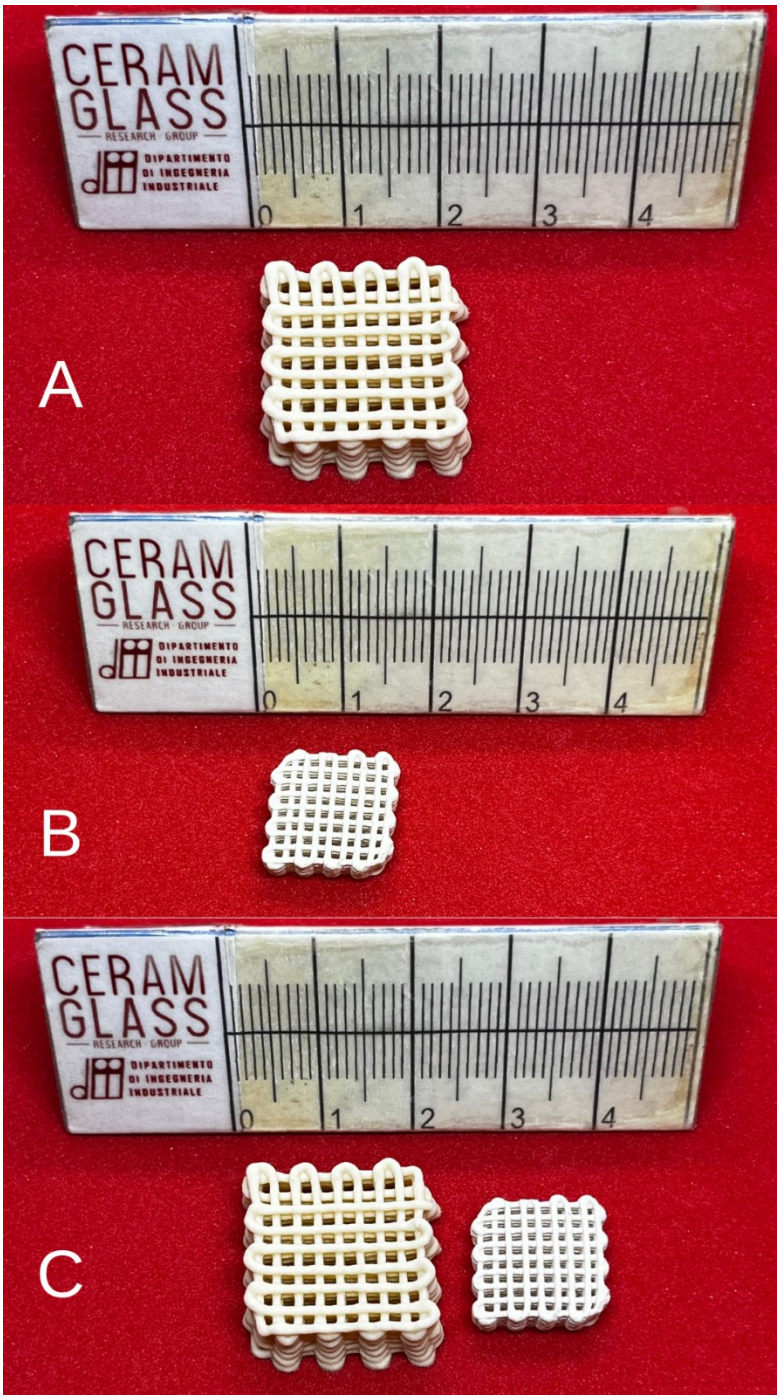

Figure 32: 1600x800 printed scaffold by calcium-nitrate tetrahydrate filler. A:1600x800 Green Scaffold; B: 1600x800 air treated scaffold at 1300°C; C: Comparison between green and air treated scaffolds

Afterwards, an attempt was made to reduce the cristobalite peak by reducing the amount of H44 to 2.69g.

Fase Oleosa	*Fase Acquosa*
2.69g H44	2.03g TiO_2
4g FunToDo	5.98g $Ca(NO_3)_2 \cdot 4H_2O$
2g Span80	10g H_2O

Table 9: Calcium Nitrate Tetrahydrate 2nd Ink formulation

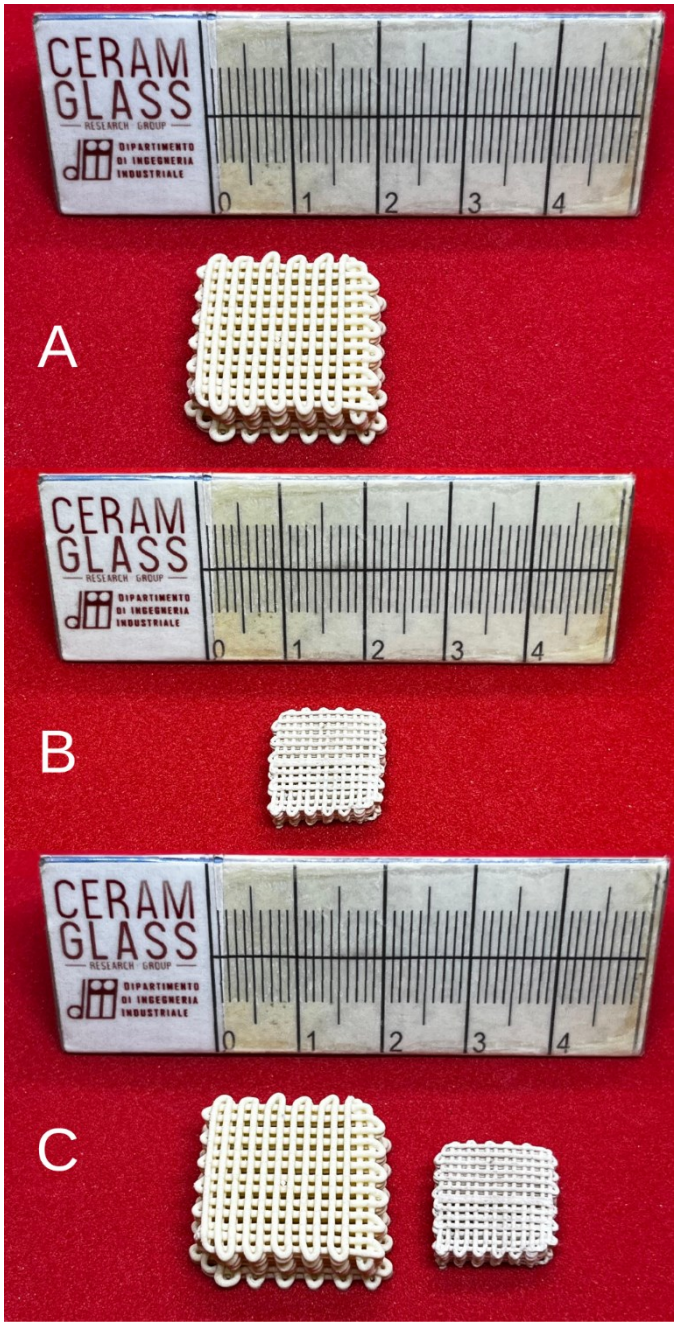

Figure 33: 800x800 printed scaffold by calcium-nitrate tetrahydrate filler. A:800x800 Green Scaffold; B: 1600x800 air treated scaffold at 1300°C; C: Comparison between green and air treated scaffolds

The volumes in percentages were obtained from the report:

$$V\ [cm^3] = \frac{m[g]}{d[\frac{g}{cm^3}]}$$

$$V[\%] = \frac{V[cm^3]}{V_{Tot}[cm^3]} \cdot 100$$

The results, for the mixture that was chosen to be characterised as showing the best results in terms of printability, are summarised in the following table.

	Density [g/cm3]	Volume [cm3]	Volume [%]
H44	0.45	6.49	23.29
FunToDo	1.05	3.81	13.68
Span80	1.00	2.00	7.18
Hexane	1.82	3.29	11.79
Calcium Nitrate Tetrahydrate	1.82	3.29	11.79
Water	1.00	10	35.90
Titania	3.89	0.52	1.87
Total	5.98	27.86	100

Table 10: Ink Materials in term of Volume

The aqueous phase appears to occupy 49.57% of the total mixture while the oily phase 52.31%. Both compositions underwent the same heat treatment, divided into four stages:

- Heating up to 500°C at a rate of 0.5°C/min
- Holding at 500°C for two hours
- Heating up to 1300°C at a rate of 5°C/min
- Holding at 1300°C for three hours
- Cooling down to room temperature at a rate of 5°C/min.

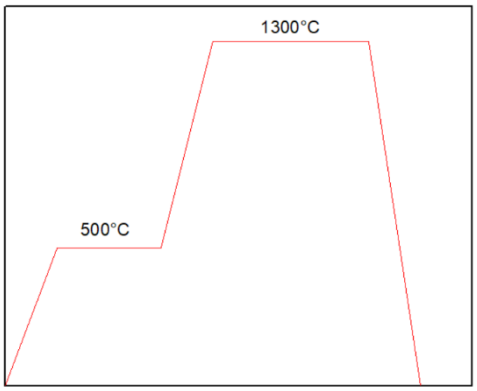

Figure 34: Schematisation of heat treatment performed

Calcite

The procedure for the formulation of the oil phase is almost identical. Difficulties were encountered in the formulation of the aqueous phase because calcite is hydrophobic and therefore insoluble in water.

Three approaches were tried, incorporating calcite in an oil phase instead of an aqueous phase, but they proved quite unsuccessful.

The fourth approach, on the other hand, responded well both in terms of printability and XRD despite being heat-treated at a higher temperature of 50°C.

- Titania was added to 8g of water and the whole was placed under ultrasound for 10 minutes to prevent the formation of agglomerates.
- Calcite was added to the mixture along with 3 drops of Span80. The whole was stirred in the Thinky for 10 min.
- 1g H_2O as added and again in the Thinky for another 10 minutes of mixing.
- An additional gram of water was added.

At this point, the aqueous phase was added to the oily phase in the same way as before, adding 1.5ml of hexane to obtain the emulsion.

Fase Oleosa	*Fase Acquosa*
2.91g H44	2.03g TiO_2
4g FunToDo	10g H_2O
2g Span80	
2.53g $CaCO_3$	

Table 11: $CaCO_3$ Ink with 10g H_2O

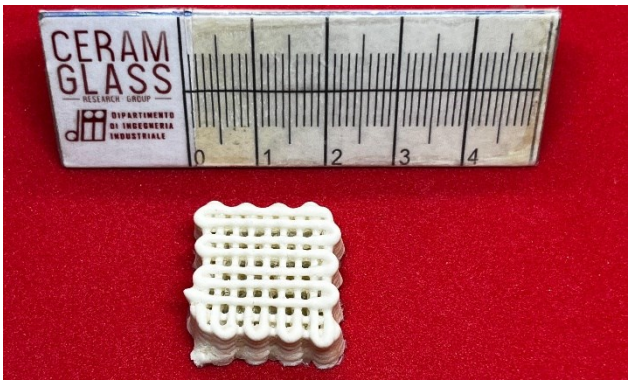

Figure 35: 800x1600 $CaCO_3$ printed scaffold with 10g H_2O Green Scaffold

Fase Oleosa	*Fase Acquosa*
2.91g H44	2.03g TiO_2
4g FunToDo	8g H_2O
2g Span80	
2.53g $CaCO_3$	

Table 12: $CaCO_3$ Ink with 8g H_2O

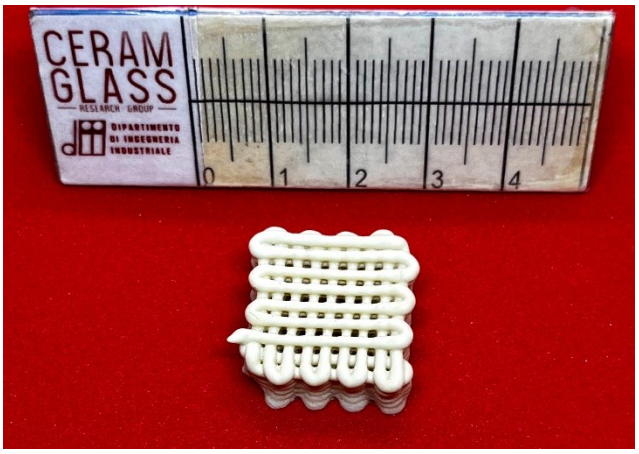

Figure 36: 800x1600 $CaCO_3$ printed scaffold with 8g H_2O Green Scaffold

Fase Oleosa	*Fase Acquosa*
2.91g H44	2.03g TiO_2
5g FunToDo	8g H_2O
2g Span80	
2.53g $CaCO_3$	

Table 13: $CaCO_3$ Ink with 5g FunToDo Resin

Figure 37: 800x1600 $CaCO_3$ printed scaffold with 5g FunToDo Resin

Fase Oleosa	*Fase Acquosa*
2.91g H44	2.03g TiO_2
4g FunToDo	8g H_2O + 2g H_2O
2g Span80	2.53g $CaCO_3$

Table 14: $CaCO_3$ Ink with $CaCO_3$ in aqueous phase

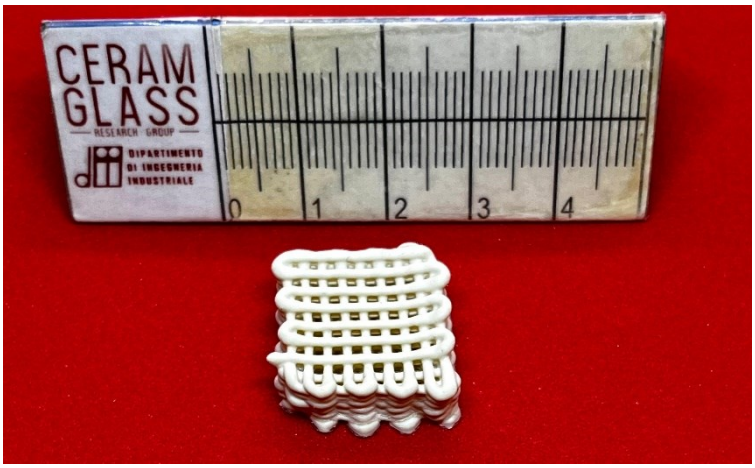

Figure 38: 800x1600 $CaCO_3$ printed scaffold with $CaCO_3$ in aqueous phase

As mentioned, two different heat treatments were used. The first was divided into four stages up to a temperature of 1300°C:

- Heating up to 500°C at a rate of 0.5°C/min
- Holding at 500°C for two hours
- Heating up to 1300°C at a rate of 5°C/min
- Holding at 1300°C for three hours

Cooling down to room temperature

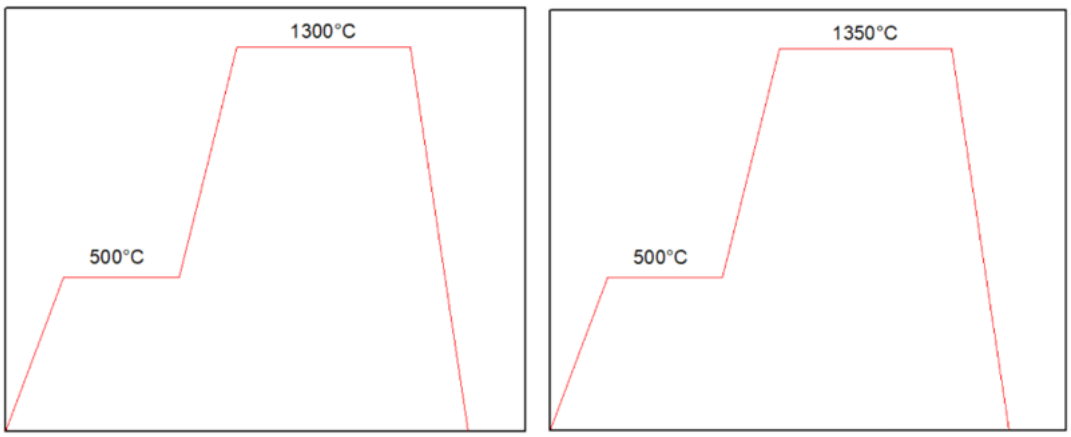

Figure 39: Heat Treatment Schematisations

Gibson-Ashby Model

Cellular materials belong to a class of materials whose porosity is their main characteristic, giving them very special mechanical properties such as lightness, energy absorption capacity and high specific strength. Thanks to these properties, the materials are widely used in many sectors ranging from construction to bioengineering.

Cellular materials consist of a continuous solid matrix that encloses pores or cavities, which may themselves be open or closed: open-cell materials have interconnected pores that allow the passage of fluids in contrast to closed-cell materials, which have cavities isolated from one another.

The mechanical properties of cellular materials are closely dependent on their structure: relative density is a critical factor since the strength and stiffness of cellular materials are generally proportional to the density of the solid matrix that constitutes them.

For closed-cell cellular materials, the compressive strength is significantly influenced by the internal pore pressure, which can contribute to improved load-carrying capacity. On the other hand, open-cell materials, such as polymer foams, show a higher energy absorption capacity due to the ability of the pores to collapse under load.

An important property of cellular materials is their ability to absorb energy through plastic deformation of the structure, which allows the material to dissipate large amounts of energy without collapsing completely.

The damping behaviour of cellular materials is also remarkable: the presence of porosity helps to reduce vibration transmission.

In the field of bone engineering, the Gibson Ashby model makes it possible to optimise the mechanical properties of scaffolds, to provide mechanical support, promote cell growth and enable the flow of nutrients to cells by promoting vascularisation.

[78, 79, 80, 81]

Model

The Gibson-Ashby Model, developed by Lorna Gibson and Michael Ashby, represents a benchmark for the analysis and design of cellular materials, being able to provide a relationship between the microstructure of the material and its macroscopic mechanical properties.

A cellular material can be imagined as a solid containing a series of cells or cavities that can themselves be open or closed: the model is able to describe how these cavities influence the overall properties of the material.

The model mainly considers two types of cellular materials:

- Open cell materials: the walls separating the pores are interconnected.
- Closed cell materials: each pore is sealed and surrounded by solid walls.

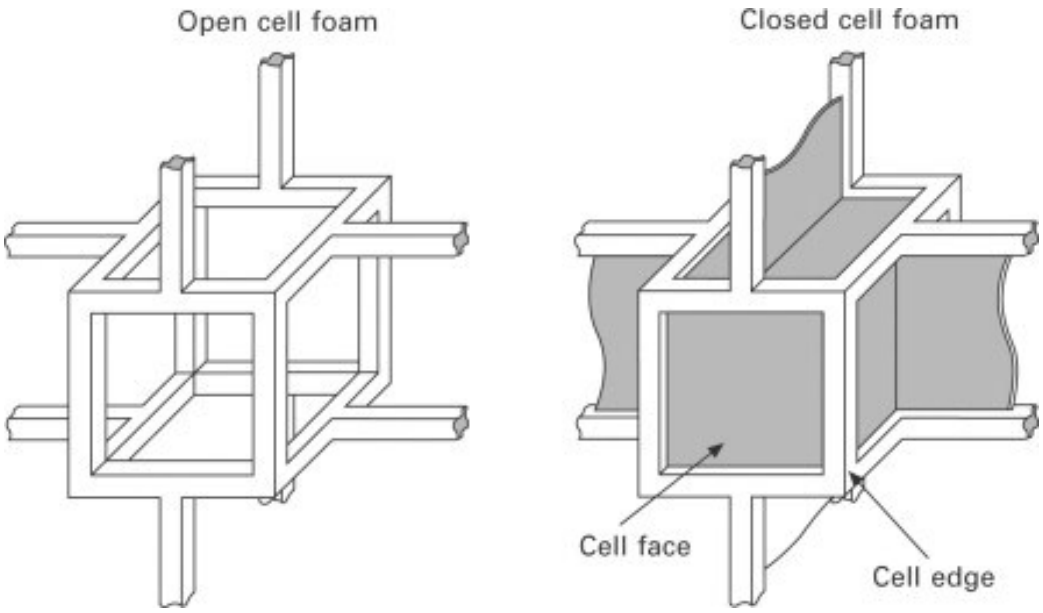

Figure 40: Open and Closed cell in Gibson-Ashby Model (XXVIII)

[82, 83, 84]

Bending-Dominated Structures

Bending-dominated structures are characterised by a mechanical response dominated by the bending of the trabeculae constituting the cells. This typically occurs in cellular materials with a complex geometry, such as foams or weakly connected lattices, in which the applied forces are not transmitted along direct lines through the structure, but rather through the bending of the walls.

The relationship linking cell size and trabecular thickness to relative density is explained by the Gibson Ashby model

$$\rho_{rel} \propto \left(\frac{t}{L}\right)^2$$

Where it is assumed that the cell size is reasonably greater than the thickness of the trabeculae.

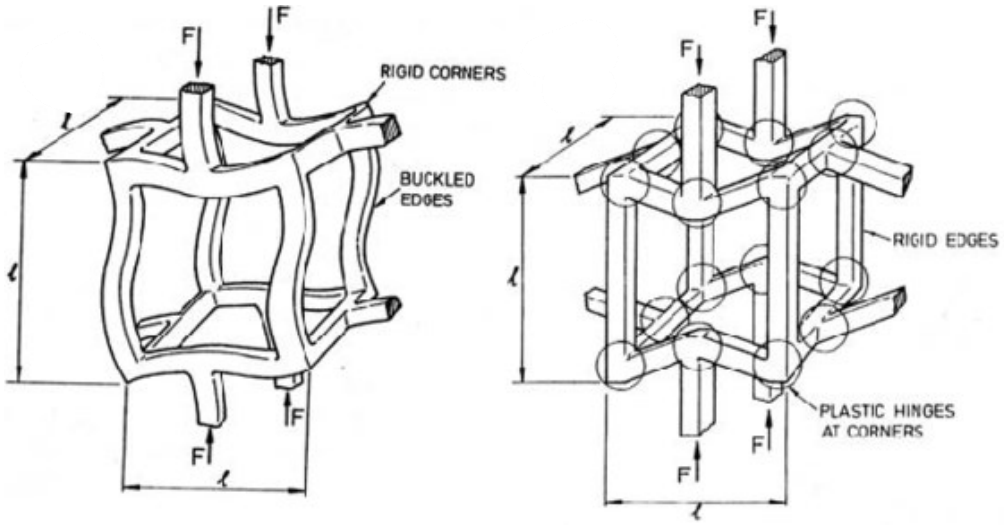

Figure 41: Bending-Dominated Structure (XXIX)

Stretch-Dominated Structures

Stretch-dominated structures are characterised by elements subjected primarily to tension and compression, rather than to bending.

The behaviour is typical of structures in which there are more connections per node so that the structure is stronger. The applied forces are distributed through the connections between the cells evenly and along optimal directions for load transmission.

Such structures are capable of bearing greater loads than bending-dominated structures, with the same density and geometry.

$$\rho_{rel} \propto \frac{\sigma_c}{\sigma_{fl,s}}$$

Where σ_c is the compressive strength and $\sigma_{fl,s}$ the bending strength of the apparent solid phase.

[85, 86]

Density

To understand whether materials comply with the model or not, it is necessary to introduce some definitions.

- Geometric Density: is the density calculated assuming the solid to be a solid parallelepiped, considering the volume in its entirety

$$\rho_G = \frac{m}{V}$$

$$V = L \cdot L \cdot h$$

- Apparent Density: is the density output by the pycnometer

$$\rho_A = \frac{m}{V_A}$$

$$V_A = V - V_{PA}$$

- Real Density: is the actual porosity of the material, obtained by excluding both open and closed porosities. Apparent density can be obtained by pulverising the sample to open porosities that were previously closed.

$$\rho_{True} = \frac{m}{V_{True}}$$

$$V_{True} = V - V_{PA} - V_{PC}$$

Ove:

m: mass of the sample [g].

ρ_G: geometry density [g/cm^3].

V: volume obtain assuming that the sample is a parallelepiped [cm^3].

ρ_A: bulk density [g/cm^3].

V_A: apparent volume obtained from the total volume deprived of open porosity [cm^3].

ρ_{True}: actual density [g/cm^3].

V_{True} actual volume obtained from the total volume stripped of open and closed porosity [cm^3]

One of the fundamental equations of the Gibson-Ashby model concerns the relationship between the relative density ρ / ρ^*_s and the elastic modulus of the cellular material E^*.

The elastic modulus of a cellular material is closely related to that of the solid material from which it is made and depends on the relative density.

In Bending-Dominated Structures:

$$E^* = C_1 \left(\frac{\rho^*}{\rho_s}\right)^2 E_s$$

In Stretch-Dominated Structures:

$$E^* = C_1 \left(\frac{\rho^*}{\rho_s}\right) E_s$$

With:

E^* elastic modulus of cellular material

E_s elastic modulus of the solid material at the base of the cellular structure

ρ^* density of the cellular material,

ρ_s density of the solid material,

C_1 constant depending on the geometry of the cell.

The relationship shows that the elastic modulus of the cellular material is directly proportional to the relative density. Cellular materials are therefore lighter and less rigid than solid solids. [71]

Mechanical Strength

The compressive strength $\sigma*$ of a cellular material is described in Bending-Dominated structures as:

$$\sigma^* = C_2 \left(\frac{\rho^*}{\rho_s}\right)^{3/2} \sigma_s$$

In Stretch-Dominated structures by:

$$\sigma^* = C_2 \left(\frac{\rho^*}{\rho_s}\right) \sigma_s$$

With:

σ^* compressive strength of cellular material

σ_s compressive strength of the solid material at the base of the cell structure,

C_2 constant depending on the geometry of the cell material.

This last equation shows how the resistance of a cellular material strongly depends on its relative density, following a power law.

Porosity

Porosity is a critical factor in cellular materials as it affects the material's ability to support cell growth and vascularisation. The size and distribution of pores must be carefully optimised: pores that are too small may hinder cell penetration, while pores that are too large may reduce the mechanical strength of the scaffold. Porosity around 60-70% and pore sizes between 100 and 500 μm are ideal for bone regeneration. The definitions of geometric density and bulk density give the following relationship:

$$\frac{V - V_{PA}}{V} = \frac{\rho_G}{\rho_A}$$

$$1 - f_{PA} = \frac{\rho_G}{\rho_A}$$

With f_{PA} open porosity fraction.

Similarly, the definitions of geometric density and real density give:

$$\frac{V - V_{PA} - V_{PC}}{V} = \frac{\rho_G}{\rho_{True}}$$

$$1 - f_{PA} - f_{PC} = \frac{\rho_G}{\rho_A}$$

With f_{PC} closed porosity fraction.

From the previous reports, it is possible to obtain:

- Open porosity as a percentage:

$$PA[\%] = f_{PA} \cdot 100$$

- Closed porosity in percent:

$$PC[\%] = f_{PC} \cdot 100$$

- Total porosity as a percentage

$$P_{Tot}[\%] = (f_{PA} + f_{PC}) \cdot 100$$

Volume Shrinkage

Volumetric shrinkage, expressed as a percentage, makes it possible to assess the discrepancy between the sample volume before and after heat treatment.

$$\Delta V\ [\%] = \left(\frac{V_i - V_f}{V_i}\right) \cdot 100$$

[85]

Mechanical Tests

Bone is a material that must withstand considerable mechanical loads, so it is essential that cellular scaffolds have adequate mechanical properties. Polymeric or ceramic materials require the support of composite materials to achieve the necessary strengths. An important challenge is to achieve an optimal balance between porosity and mechanical strength: high porosity promotes bone regeneration but reduces the strength of the material.

Compression Tests

Compression tests were carried out to assess the strength of the samples. The procedure involves first measuring the cross-section of the samples: this will be entered into the programme for the evaluation of the strength itself.

The values obtained were used to derive the compressive strength σ_C which in turn allowed the $\sigma_{f,s}$ to be obtained:

$$\sigma_{f,s} = \frac{5\sigma_c}{(\rho_{rel})^{1.5}}$$

$$\rho_{Rel} = 1 - \rho_{Tot}$$

[86]

Chapter 5

Results

This chapter will analyse the results obtained through experiments aimed at obtaining sphene from two calcic precursors: calcium nitrate tetrahydrate and calcite.

The two compositions will be analysed based on multiple factors: XRD analysis, porosity measurement, optical and electron microscopy, taking into account the criticalities found during the process. Subsequently, the results obtained from the mechanical tests will be discussed.

Mechano-physical Characterization

The research started with the evaluation of two types of ink obtained from different calcium sources: calcium nitrate tetrahydrate and calcite ($CaCO_3$). This section will evaluate the quality of the scaffolds, commenting on the observations obtained by microscopy, XRD analysis and the porosity of the samples, referring to both green and heat-treated samples. Let us now look in detail at the compositions and scaffolds obtained.

Calcite

The most critical issues were encountered in the preparation of the calcite-based ink as this, which was originally supposed to make up the aqueous phase together with titania, turned out to be highly hydrophobic. Several tests were carried out, on several formulations, to improve printing but without success as phase separation was more than evident in each attempt. The scaffolds were printed by direct ink writing, using a 0.84mm nozzle following a path implemented by means of two g-code files

- 800 x 1600 with a line spacing of 240µm
- 800 x 800 with a line spacing of 1600µm

$CaCO_3$: 1st Ink

The quantities of powder used in this mixture were obtained from the stoichiometry of sphene $CaTiSiO_5$.

It is desired to obtain:

$$g\ SiO_2 + g\ TiO_2 - g\ CaO = 5g$$

The molar mass (MM) of all the oxides required to form sphene is then calculated.

- Titania TiO_2

$$MM_{TiO_2} = 47{,}88 + 2(15{,}999) = 79{,}87 g/mol$$

- Silicon dioxide SiO_2

$$MM_{SiO_2} = 22{,}085 + 2(15{,}999) = 60{,}083 g/mol$$

Calcium oxide CaO

$$MM_{CaO} = 40{,}078 + 15{,}99 = 56{,}077 g/mol$$

From the molar masses, the quantity in grams is derived:

$$g = n \cdot MM$$

Since the ratios are 1:1:1, we have that:

$$\frac{n°\ moles\ TiO_2}{n°\ moles\ SiO_2} = 1 = \frac{g\ TiO_2}{MM\ TiO_2} \cdot \frac{MM\ SiO_2}{g\ SiO_2}$$

$$g\ TiO_2 = g\ S_iO_2 \cdot \frac{MM\ T_iO_2}{MM\ S_iO_2} = gSiO_2 \cdot 1.33$$

$$g\ CaO = g\ S_iO_2 \cdot \frac{MM\ T_iO_2}{MM\ S_iO_2} = gSiO_2 \cdot 0.43$$

Setting up a system:

$$\begin{cases} g\ SiO_2 + g\ TiO_2 - g\ CaO = 5g \\ g\ TiO_2 = g\ SiO_2 \cdot 1.33 \\ g\ CaO = g\ SiO_2 \cdot 0.43 \end{cases} \rightarrow \begin{cases} gSiO_2 = 1.53g \\ g\ TiO_2 = 2.03g \\ g\ CaO = 1.42g \end{cases}$$

Evaluating the performance of the compounds at our disposal:

- H44 has a yield of 52.5%

$$g\ SiO_2 = 0{,}525g\ H44 \rightarrow g\ H44 = \frac{g\ SiO_2}{0.525} = 2.91g$$

- TiO_2 has a yield of 99,9%

$$g\ TiO_2 = 0{,}999g\ HTiO_2 \rightarrow g\ TiO_2 = \frac{g\ TiO_2}{0.999} = 2.03g$$

- Calcite is in a 1:1 ratio with calcium oxide

$$MMCaCO_3 = 100{,}086\ g/mol$$

$$\frac{g\ CaCO_3}{g\ CaO} = \frac{MM\ CaCO_3}{MM\ CaO} = \frac{100{,}086}{56{,}077} \rightarrow g\ CaCO_3 = 1.78g\ CaCO_3 = 2{,}53g$$

Fase Oleosa	*Fase Acquosa*
2.91g H44	2.03g TiO_2
4g FunToDo	10g H_2O
2g Span80	
2.53g $CaCO_3$	

Table 15: $CaCO_3$ Ink with quantities dictated by stoichiometry

As mentioned in the previous chapter, the scaffolds were printed using Delta WASP 2040 PRO: the pattern used in this formulation was 800 x 1600 with a line spacing of 2400µm.

The sintering of this type of scaffold was carried out by heat treatment at 1300°C. The graph obtained by XRD is reported.

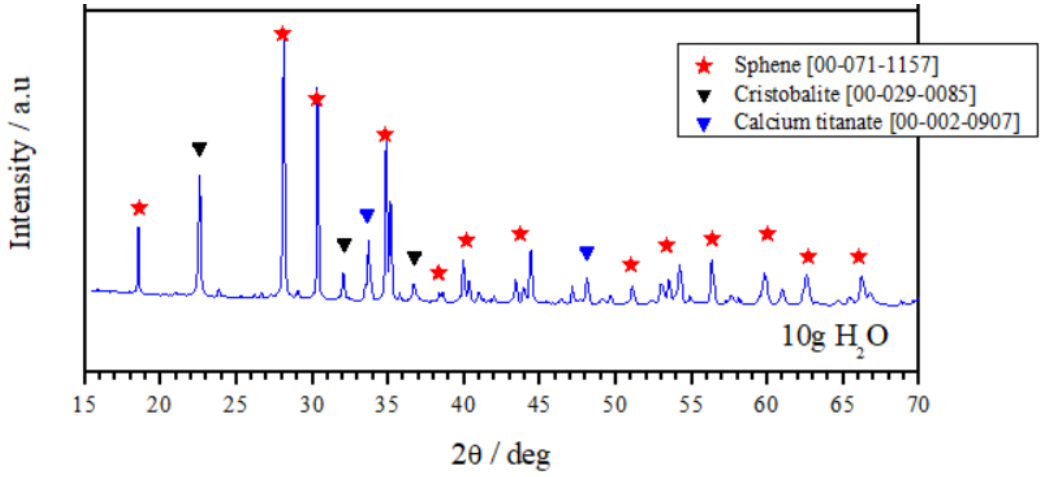

Figure 42: X-ray diffractometry of 1st Ink made of $CaCO_3$ with 10g H_2O

The presence of cristobalite is due to silicon oxide not participating in the formation of the sphene lattice. For this reason, other formulations were tested.

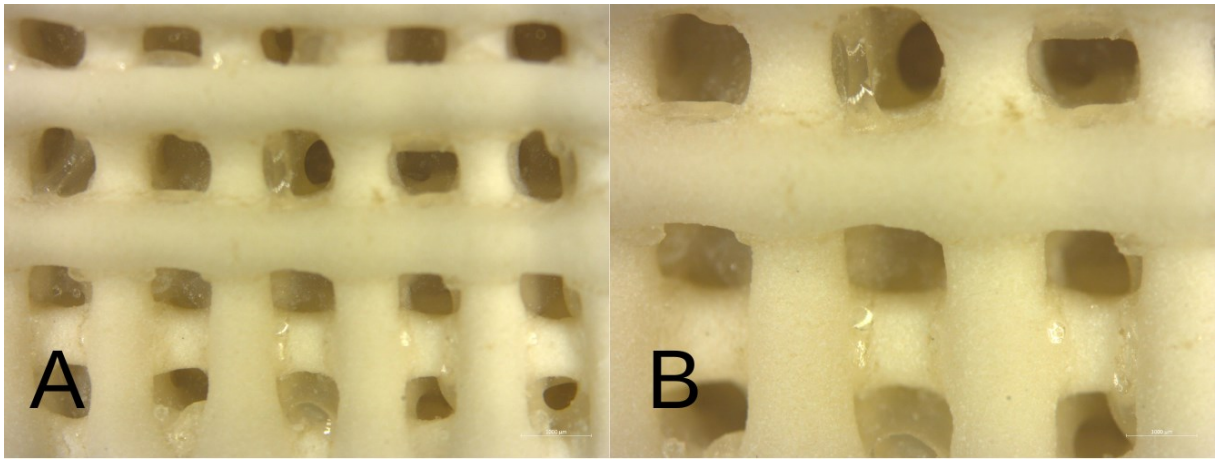

Figure 43: Scaffolds 1600x800 made of 1st Ink $CaCO_3$ characterisation under stereomicroscopy. A: green body at lower magnification; B: green body at high magnification

Images obtained by stereomicroscopy show the poor quality of the moulding: the scaffolds exhibited obvious phase separation due precisely to the difficulty of calcite interacting with the aqueous phase.

$CaCO_3$: 2nd Ink

The second attempt was achieved by reducing the amount of water in the aqueous phase.

Fase Oleosa	*Fase Acquosa*
2.91g H44	2.03g TiO_2
4g FunToDo	8g H_2O
2g Span80	
2.53g $CaCO_3$	

Table 16: 2nd Ink Composition with $CaCO_3$ Filler

Despite the clear improvement in print, also confirmed by XRD analysis, phase separation persists.

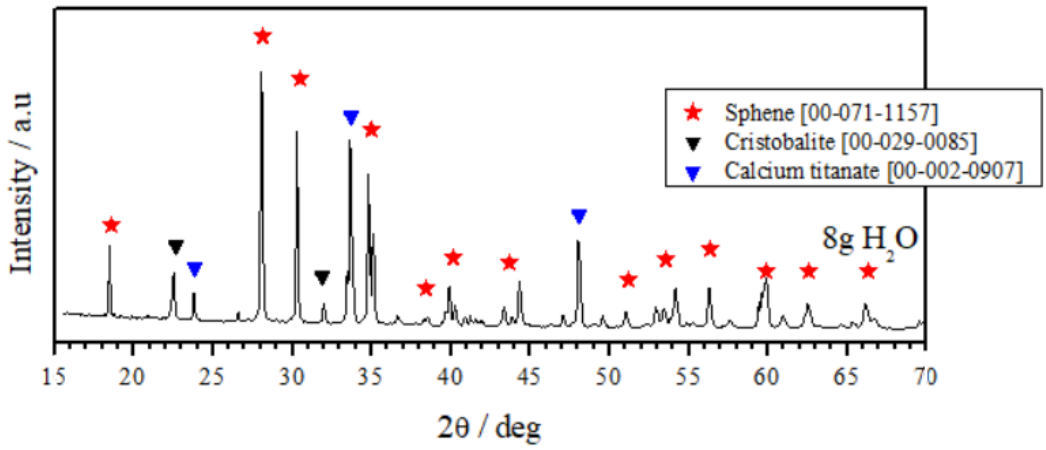

Figure 44: X-ray diffractometry of 2nd Ink made of $CaCO_3$ with 8g H_2O

Despite this, a decrease in cristobalite peaks can be observed.

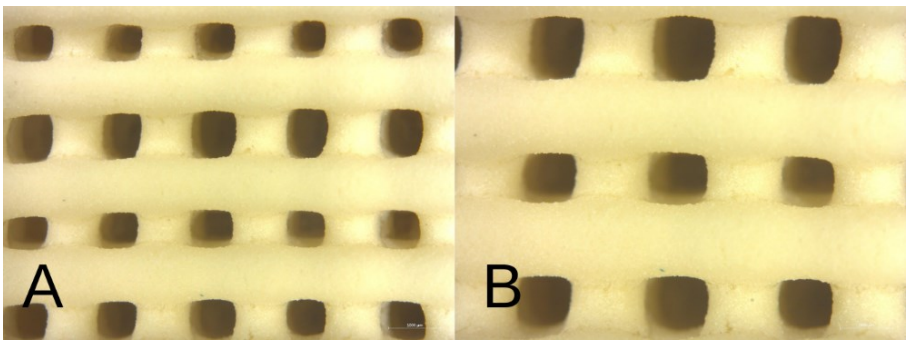

Figure 45: Scaffolds 1600x800 made of 2nd Ink $CaCO_3$ characterisation under stereomicroscopy. A: green body at lower magnification; B: green body at high magnification

$CaCO_3$: 3rd Ink

Oily Phase	*Aqueous Phase*
2.91g H44	2.03g TiO_2
5g FunToDo	8g H_2O
2g Span80	
2.53g $CaCO_3$	

Table 17: 3rd Ink Composition with $CaCO_3$ Filler

In order to improve the dispersion of the calcite particles, a further attempt was made by increasing the amount of FunToDo resin by one gram from 4g to 5g.

In this way, however, the phase separation was even more pronounced.

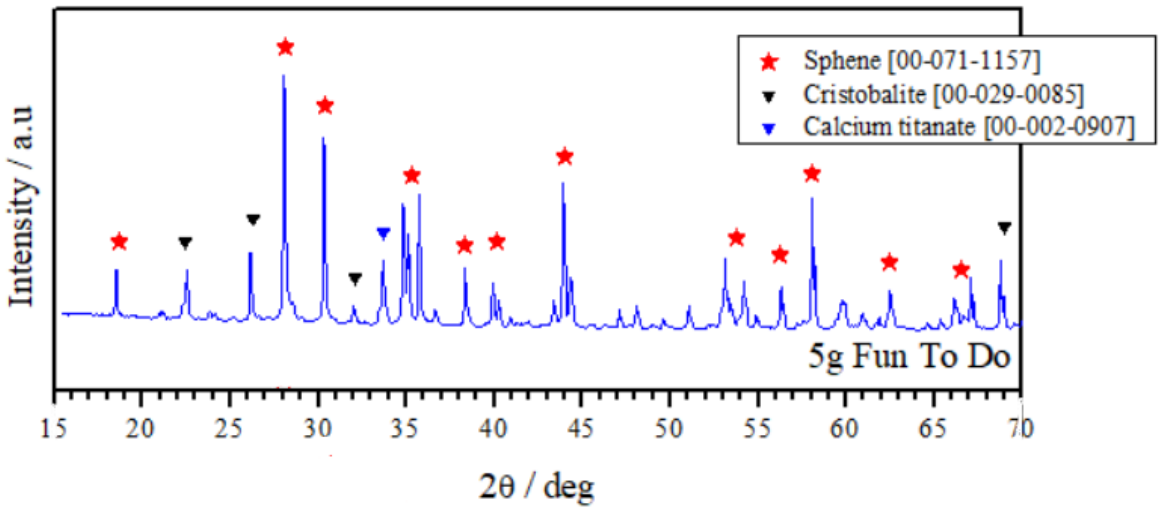

Figure 46: X-ray diffractometry of 3rd Ink made of $CaCO_3$ with 5g of FunToDo Resin

$CaCO_3$: 4th Ink

The final attempt was achieved with a different process, trying to dissolve calcite in the aqueous phase using Span80 a surfactant.

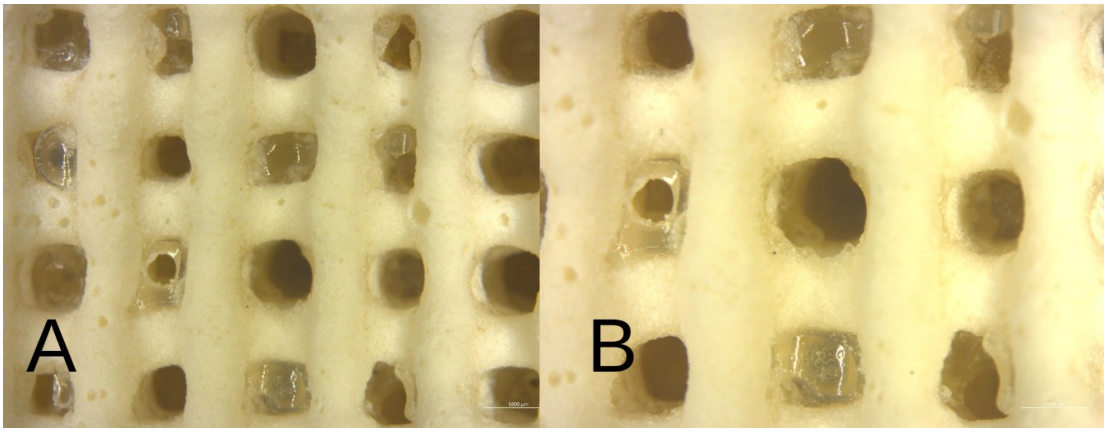

Figure 47: Scaffolds 1600x800 made of 3rd Ink $CaCO_3$ characterisation under stereomicroscopy. A: green body at lower magnification; B: green body at high magnification

The process involves formulating the oily phase by dissolving H44 in transparent silicone resin FunToDo overnight.

The next day, Span80 is added and then the oily phase is placed under mechanical agitation.

We proceed with the formulation of the aqueous phase in 3 steps:

- Step 1: Titania is dissolved in 8g water and subjected to ultrasonic magnetic stirring for 10 minutes.
- Step 2: calcite is added to the aqueous phase and 3 drops of Span80 and 1g of water are added.

  This is placed in an orbital mixer at a speed of 2200 rpm for 10 minutes.
- Step 3: Following the addition of a further gram of water, the aqueous phase is combined with the oily phase and left under mechanical stirrer for 20 min.

This is followed by the addition of 1.5ml of n-hexane to promote emulsification and printing.

Two types of scaffolds were printed by this process:

- 800 x 1600 with a line spacing of 2400µm
- 800 x 800 with a line spacing of 1600µm

This confirmed the stability of the emulsion obtained, despite the phase separation that unfortunately remains. For these scaffolds, a heat treatment at 1350°C was performed, which resulted in higher purity than previous attempts.

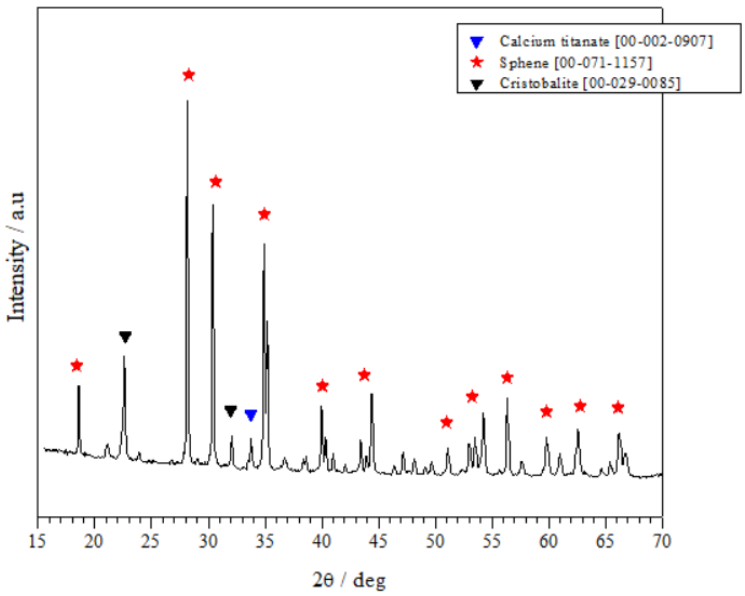

Figure 48: X-ray diffractometry of 4th Ink made with $CaCO_3$ in aqueous phase

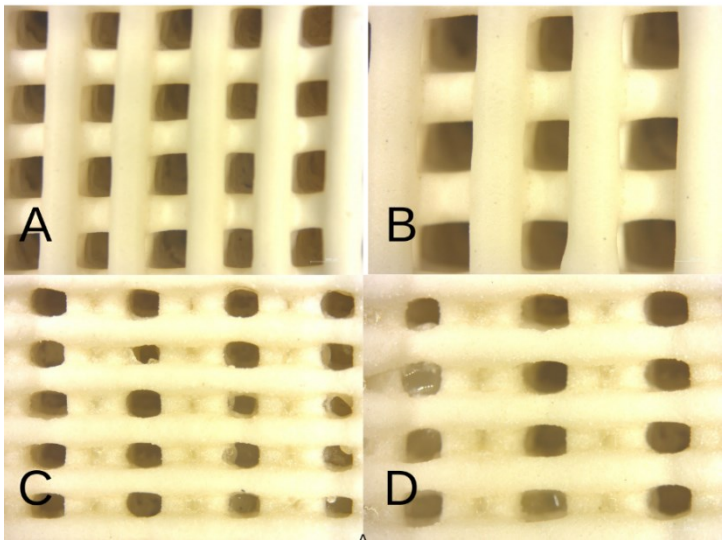

Figure 49: Scaffolds 1600x800 made of 4th Ink $CaCO_3$ characterization under stereomicroscopy. A: green body at lower magnification; B: green body at high magnification.
Scaffolds 800x800 made of 4th Ink $CaCO_3$ characterization under stereomicroscopy. C: green body at lower magnification; D: green body at high magnification.

Amount of Water

Although it was not possible to obtain 100% pure sphene, the characterisation of the scaffolds by XRD analysis made it possible to compare the formulations performed.

Because of these analyses, all subsequent mixture modifications were made.

A first comparison can be made on the amount of water within the composition.

The reduction in water made it possible to obtain more printable scaffolds but also a decrease in the cristobalite peak, distinguishable at 23° at the expense of the increase in calcium titanate peaks, at 24°, 34° and 48°, with the same heat treatment.

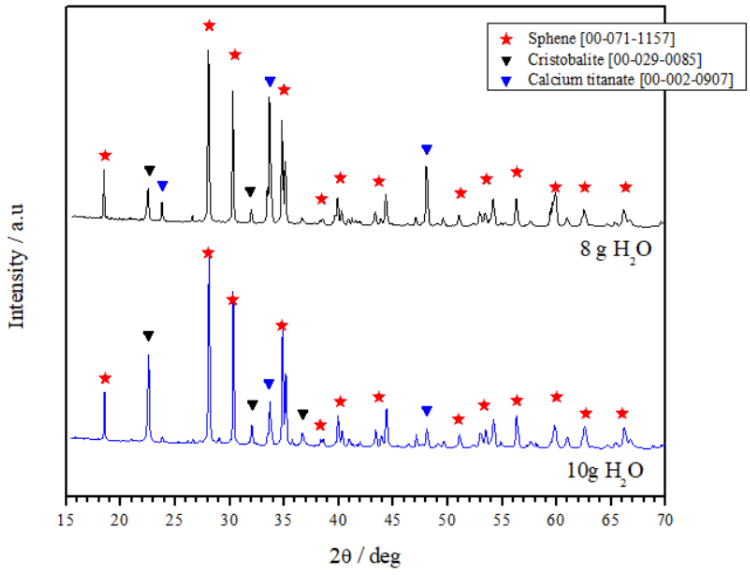

Figure 50: Comparison between ink made of $CaCO_3$ with different amount of Water, 8 g (up) and 10 g (down)

The presence of unwanted phases, however, is not an insurmountable problem as both cristobalite and calcium titanate are able to promote osseointegration.

Amount of Resin

A second comparison considers the amount of transparent silicone resin used (FunToDo).

Although this resin does not improve the mouldability of the scaffolds, it almost eliminated the calcium titanate phase, favouring the appearance of more cristobalite peaks at 24°, 27° and 33°.

Note also how the XRD analysis in the case of mixing with 5g resin favoured the appearance of sphene peaks.

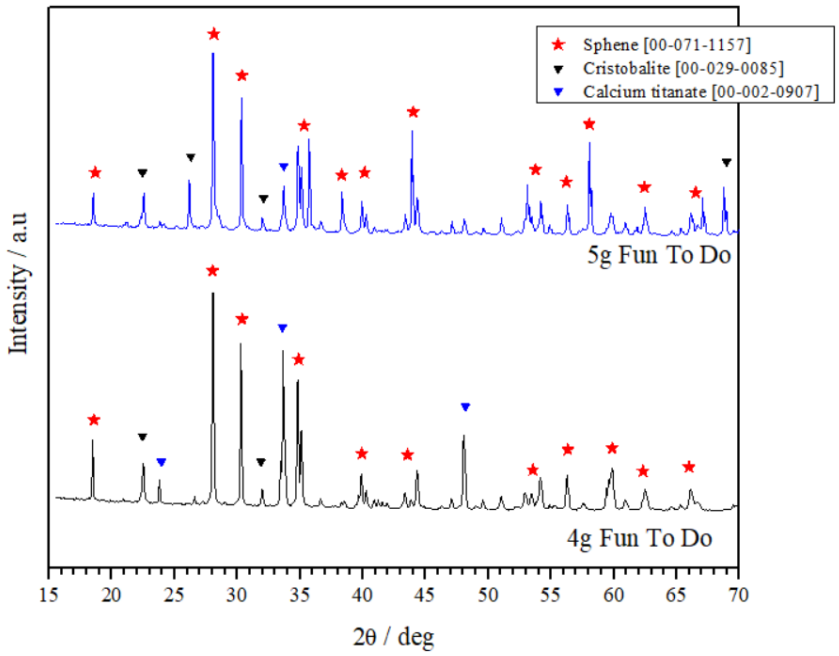

Figure 51: Comparison between ink made of $CaCO_3$ with different amount of FunToDo Resin 5g (up) and 4g (down)

This is due precisely to the calcite which, being more soluble in resin than in water, was able to bond with titania and silicon oxide rather than oxygen to form titanate.

Unfortunately, however, this choice largely compromised printability, as the scaffolds exhibited bubbles and other imperfections in addition to phase separation.

For this reason, it was decided to continue the formulation while keeping the amount of transparent resin at 4 g.

Sintering

Also want to compare the first and the last attempt, which underwent the same heat treatment but at different temperatures.

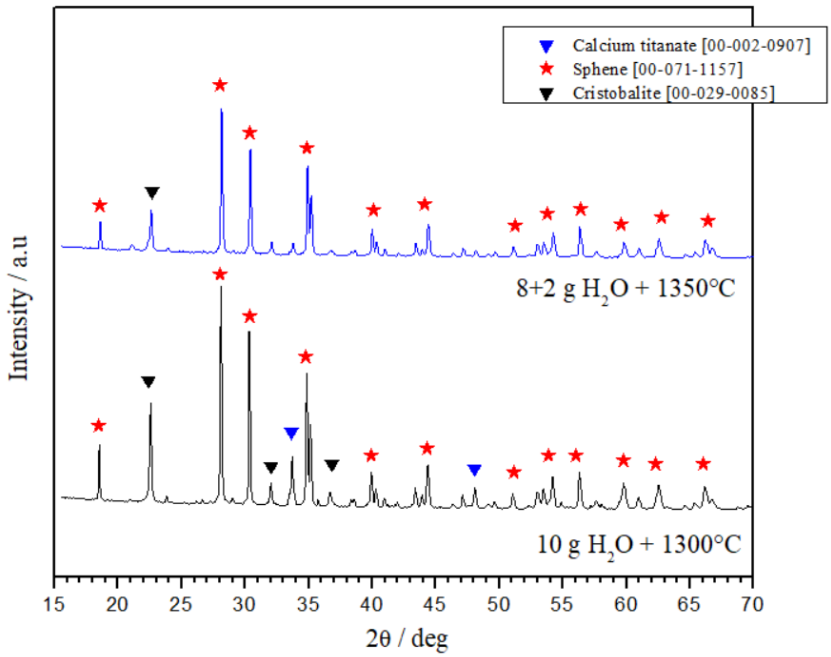

Figure 52: Comparison between ink made of $CaCO_3$ sintered at 1350°C (up) and 1300°C (down)

Note how the higher temperature, coupled with a process in which the calcite is in the aqueous phase, made it possible to obtain almost completely pure sphene, despite the cristobalite peak that was impossible to eliminate.

In fact, the fourth ink is the one with the best formulation: the calcite was included in the aqueous phase, dispersing with no little difficulty, also making printability better than in the other formulations.

Unfortunately, it was not possible to avoid phase separation, especially in the first extruded filaments, making the print still inaccurate.

Porosity and Density Measurements

The density measurements of the green samples are shown in the following table.

Model	Volume [cm^3]	Mass [g]	ρG ±DS [g/cm^3]	ρA±SD [g/cm^3]	ρR±SD [g/cm^3]	PA
800x1600 1st Ink	1.545	1.445	0.98 ±0.211	1.54 ±0.010	0.64 ±0.142	35.82
800x1600 2nd Ink	1.495	1.719	1.14 ±0.101	1.75 ±0.204	0.66 ±0.019	34.40
800x1600 3rd Ink	2.065	2.037	1.02 ±0.178	1.49 ±0.009	0.69 ±0115	31.31
800x1600 4th Ink	1.665	1.547	0.94 ±0.085	1.5 ±0.027	0.63 ±0.04	37.28
800x800 4th Ink	2.13	1.799	0.84 ±0.012	1.51 ±0.004	0.56 ±0.009	44.09

Table 18: A comparison between measurements of Density and Porosity in Green scaffolds made of Sphene from $CaCO_3$

Even though the porosity values obtained for the 1600x800 scaffolds do not match the model (73%), it should be noted that 4th ink obtained the best results of all the mixtures tested.

Also, for the 800x800 scaffolds, the porosity value obtained is far from that of the model (60%) but much closer than the values obtained in the other models.

This discrepancy is most likely due to the phase separation that occurred during Direct Ink Writing.

Calcium nitrate tetrahydrate

Here too, a couple of tests were made from the stoichiometry of sphene to achieve a high degree of purity.

The printing methods are the same as with calcite: direct ink writing in which the filament, extruded from a 0.84 mm nozzle, follows two types of paths:

- 800 x 1600 with a line spacing of 2400µm
- 800 x 800 with a line spacing of 1600µm

Calcium-Nitrate Tetrahydrate: 1st Ink

For the formulation of mixtures, the starting point is again the stoichiometry whose calculations have already been commented on.

The only difference in composition is due to the use of calcium nitrate tetrahydrate which, like calcite is in a 1:1 ratio with calcium oxide:

$$MM(Ca(NO_3)_2 \cdot 4H_2O = 236{,}146 g/mol$$

$$\frac{g\ (Ca(NO_3)_2 \cdot 4H_2O}{g\ CaO} = \frac{MM\ (Ca(NO_3)_2 \cdot 4H_2O}{MM\ CaO} = \frac{236{,}146}{56{,}077} \rightarrow g\ (Ca(NO_3)_2 \cdot 4H_2O$$
$$= 1.78g\ (Ca(NO_3)_2 \cdot 4H_2O = 5{,}98g$$

Oily Phase	*Aqueous Phase*
2.91g H44	2.03g TiO_2
4g FunToDo	5.98g $Ca(NO_3)_2 \cdot 4H_2O$
2g Span80	10g H_2O

Table 19: 1st Ink Composition with Calcium-Nitrate Tetrahydrate Filler

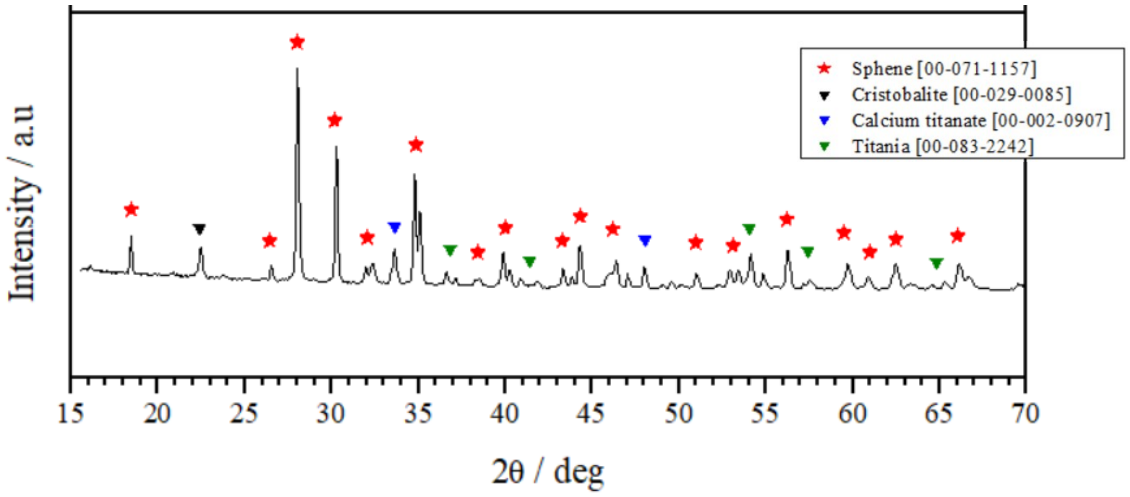

Figure 53: X-ray diffractometry of 1st Ink made of Calcium-Nitrate Tetrahydrate with 2.91g Silres®H44 respecting the stoichiometry of Sphene

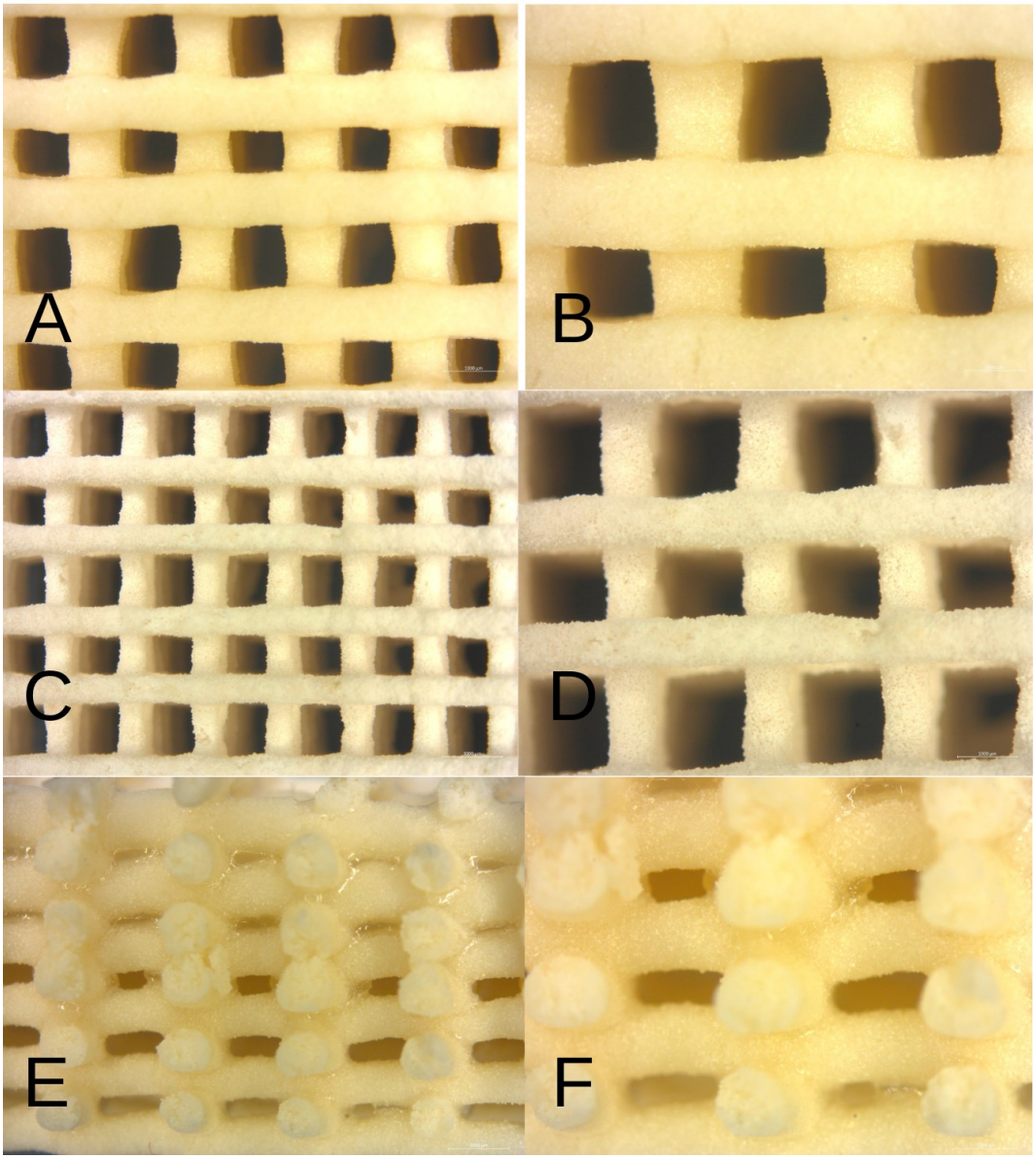

Figure 54: Scaffolds 1600x800 made of 1st Ink Calcium-Nitrate Tetrahydrate characterization under stereomicroscopy. A: green body at lower magnification; B: green body at high magnification; C: Air treated sample after 1300°C sintering at low magnification; D: Air treated sample after 1300°C sintering separation at lower magnification; F: Cut section at high magnification

Calcium-Nitrate Tetrahydrate: 2nd Ink

Oily Phase	*Aqueous Phase*
2.69g H44	2.03g TiO_2
4g FunToDo	5.98g $Ca(NO_3)_2 \cdot 4H_2O$
2g Span80	10g H_2O

Table 20: 2nd Ink Composition with Calcium-Nitrate Tetrahydrate Filler

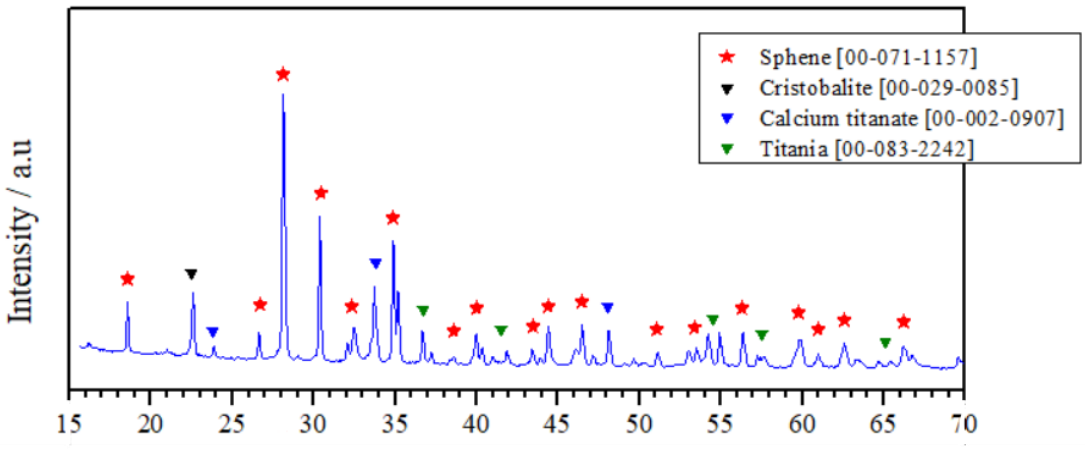

Figure 55: X-ray diffractometry of 2nd Ink made of Calcium-Nitrate Tetrahydrate with 2.69g Silres®H44

The second ink test was carried out to reduce the visible cristobalite peak to 23°.

A 7.5% reduction of H44 was tested, which did not favour the elimination of the cristobalite peak but did favour the appearance of a visible calcium titanate peak at 24°.

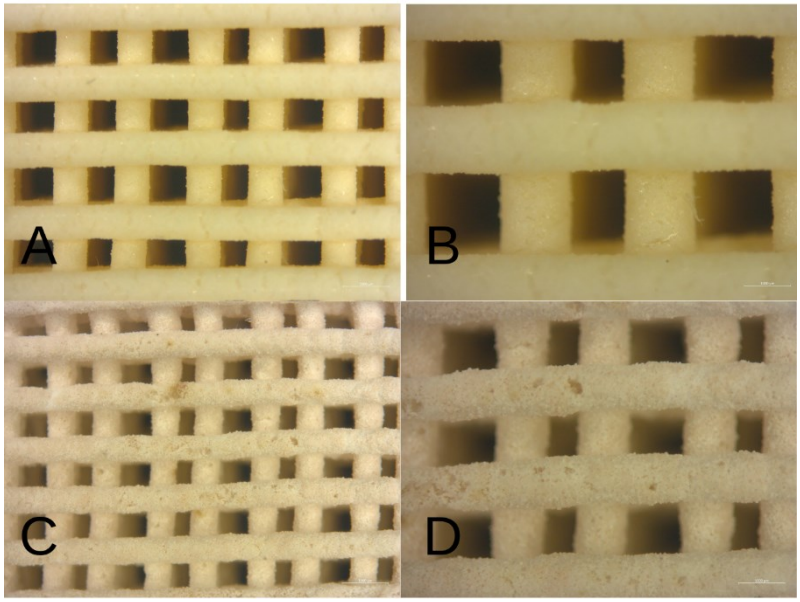

Figure 56: Scaffolds 800x800 made of 2nd Ink Calcium-Nitrate Tetrahydrate characterization under stereomicroscopy. A: green body at lower magnification; B: green body at high magnification; C: Air treated sample after 1300°C sintering at low magnification; D: Air treated sample after 1300°C sintering at high magnification

Amount of H44

The investigation of the amount of H44 was carried out to understand its role in the occurrence of the cristobalite peak.

To do this, two mixtures were tested that differed only in the amount of H44 present within: 2.91g versus 2.69g.

However, to the detriment of expectations, this solution did not lead to any improvement, so it was decided to continue with the 2.91g H44 ink.

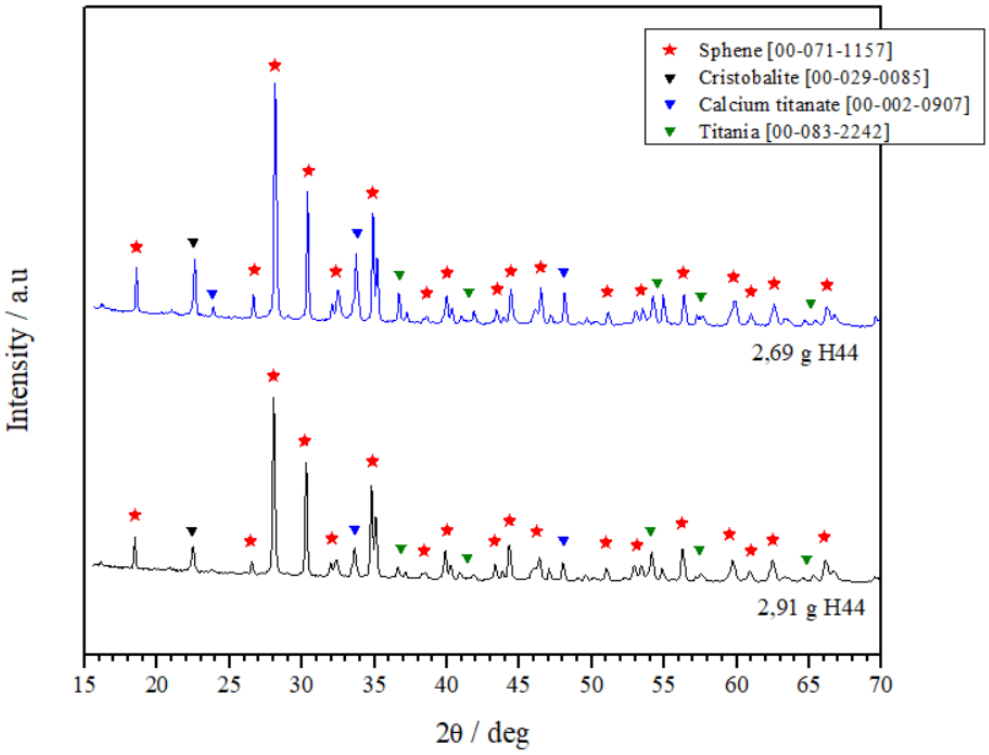

Figure 57: Comparison between ink made of Calcium-Nitrate Tetrahydrate with different amount of Silres®H44

Mixing Time

To understand what factors influenced the purity of the composition, mixing times were also analysed.

The comparison was made with three inks mixed for 10, 20 and 30 minutes respectively.

This test was carried out to understand whether the dispersion of the powders within the resin the cause of the absence of a pure sphene phase was.

As the X-ray analysis showed, the increase in mixing time did not clearly affect the crystalline phases within the ceramic compound.

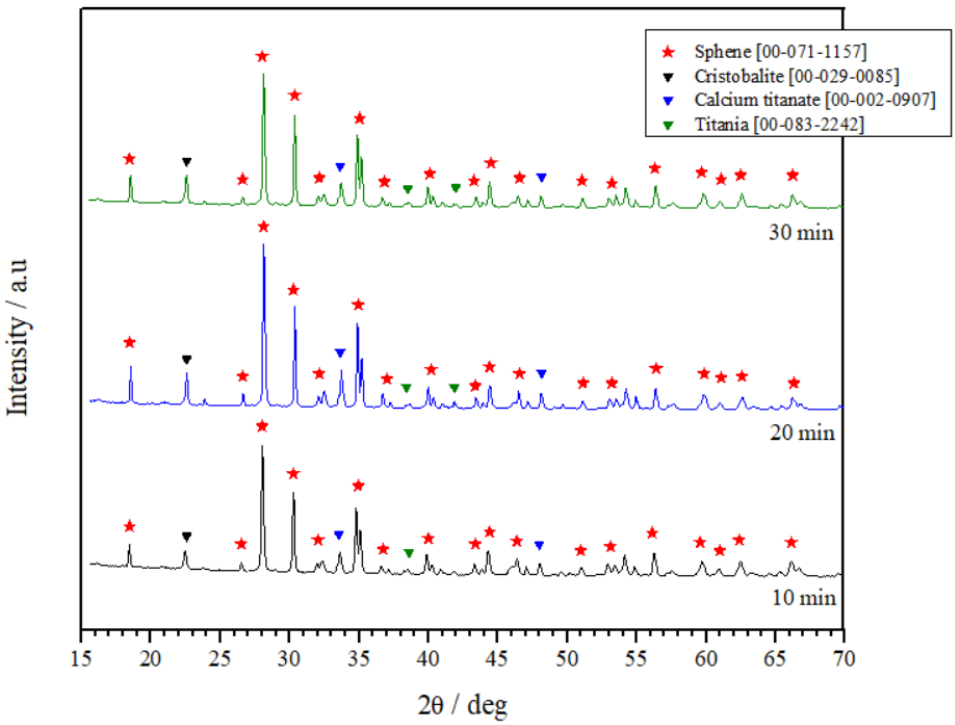

Figure 58: Comparison between different mixing times in Calcium-Nitrate Tetrahydrate Ink

Heat treatment

Again, two types of heat treatment were carried out, differing not in temperature but in treatment time.

A comparison was made between the heat treatment performed for 3 hours at 1300°C and the treatment performed for 5 hours.

No significant differences were found, so it was decided to continue the experiment with the 3-hour treatment.

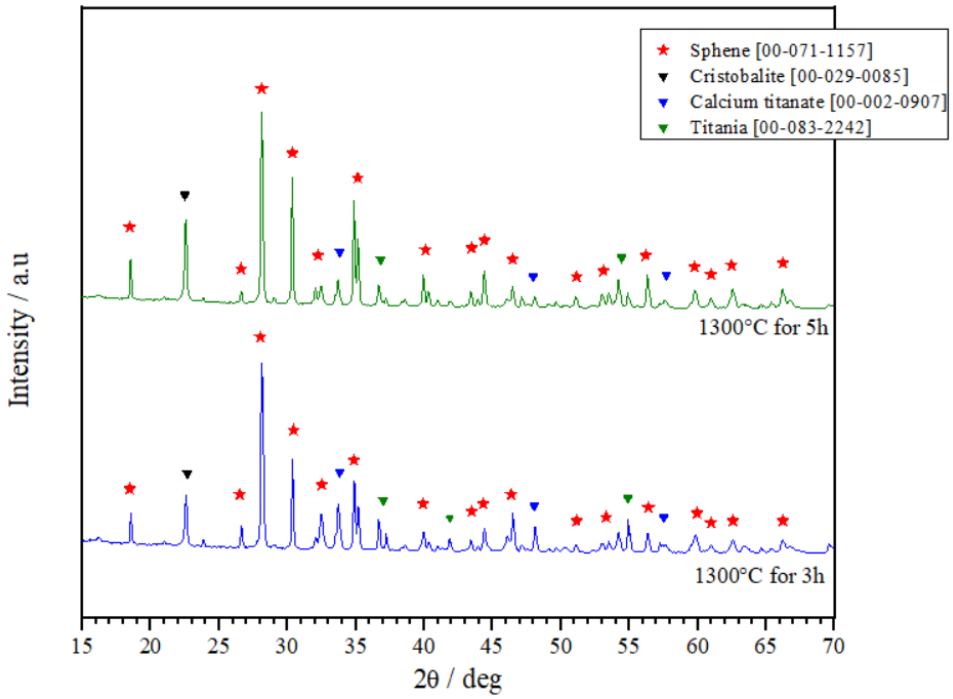

Figure 59: Comparison between different heat process in Calcium-Nitrate Tetrahydrate Ink

Porosity and Density Measurements

The density and porosity measurements for sphene scaffolds with Calcium-Nitrate Tetrahydrate as precursor are shown in the table below.

Model	Volume [cm^3]	Mass [g]	ρG ±DS [g/cm^3]	ρA±SD [g/cm^3]	ρR±SD [g/cm^3]	PA [%]	PT [%]
			Real Density	Apparent Density	Relative Density	Open Porosity	Total Porosity
800x1600 Green	2.594	1.688	0.66 ±0.100	1.51 ±0.040	0.44 ±0.069	56.46	-
800x1600 AirTreated	0.794	0.409	0.51 ±0.045	3.34 ±0.126	0.15 ±0.012	84.65	84.73

Table 21: A comparison between measurements of Density and Porosity in Green and Air-treated scaffolds made of Sphene from Calcium-Nitrate Tetrahydrate.

Although the porosity of the green scaffolds is 56.46% and is on average lower than that expected by the model which is 73%, the porosity values of the treated scaffolds exceed the apparent density expected by the model by 80%.

The low porosity of the pre-treatment scaffold could be attributed to the incorrect extrusion of the material which, due to the presence of air in the syringe, was not properly deposited.

Despite this, following heat treatment the increase in porosity is evident: the causes can be attributed to the conversion phase from polymeric to ceramic product.

Mechanical Tests

The compression tests served to mechanically characterise the material. This, after being measured, was placed under a press by which the compressive strength and apparent flexural strength could be measured.

These tests revealed the 'spongy' behaviour of the material, which, despite its low compressive strength mainly due to the high porosity of the material itself, is able to absorb energy during compression due to the gradual collapse of the pores.

Model	PT [%]	ρ_{rel}	σ_c [MPa]	$\sigma_{f,c}$ [MPa]
	Total Porosity	Relative Density	Compressive strength	Flexural strength apparent solid phase
800x1600 Air Treated	84.73	3.34 ±0.126	0.27 ±0.036	22.56

Table 22: Mechanical and Flexural Strength of scaffold made of Sphene from Calcium-Nitrate Tetrahydrate

Microstructural characterization

To conclude the characterisation, electron microscopy analyses were carried out on a scaffold obtained from calcium nitrate tetrahydrate, treated at 1300°C.

From the images, the scaffold retained the typical cell structure of the material.

It can be seen that the scaffold is very similar to trabecular bone tissue from a microstructural point of view, but not only. They share important characteristics that are evaluated below.

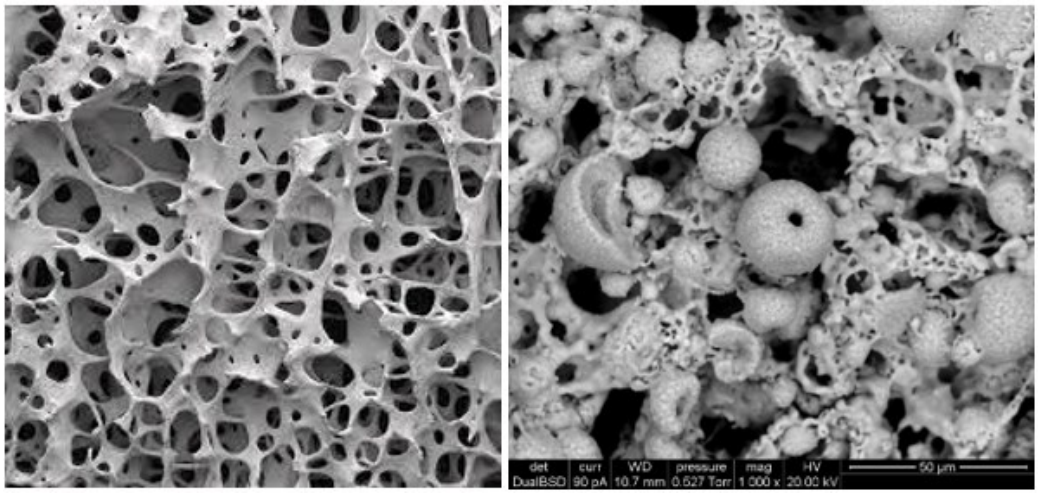

Figure 60: Comparison of trabecular bone tissue and scaffold microstructure

Porous Structure

Trabecular bone has a highly porous structure that allows adequate load distribution but also the exchange of nutrients and waste substances.

The porosity of the material obtained mimics the bone very well, allowing vascularisation and the growth of new tissue that will replace the scaffold.

Bone tissue growth support

The trabeculae offer mechanical support and facilitate the activity of osteoblasts (and osteoclasts, promoting bone remodelling and regeneration.

Being bio-compatible, the sphene scaffold is designed to promote cell colonization and bone matrix deposition, acting as a "scaffold" on which new bone tissue can grow.

Interaction with surrounding tissue

Due to its open structure and bone cell activity, trabecular bone can continuously interact with surrounding tissues, promoting regeneration and remodelling processes. Again, the bioactivity of the sphene can stimulate cell adhesion by promoting mineralisation.

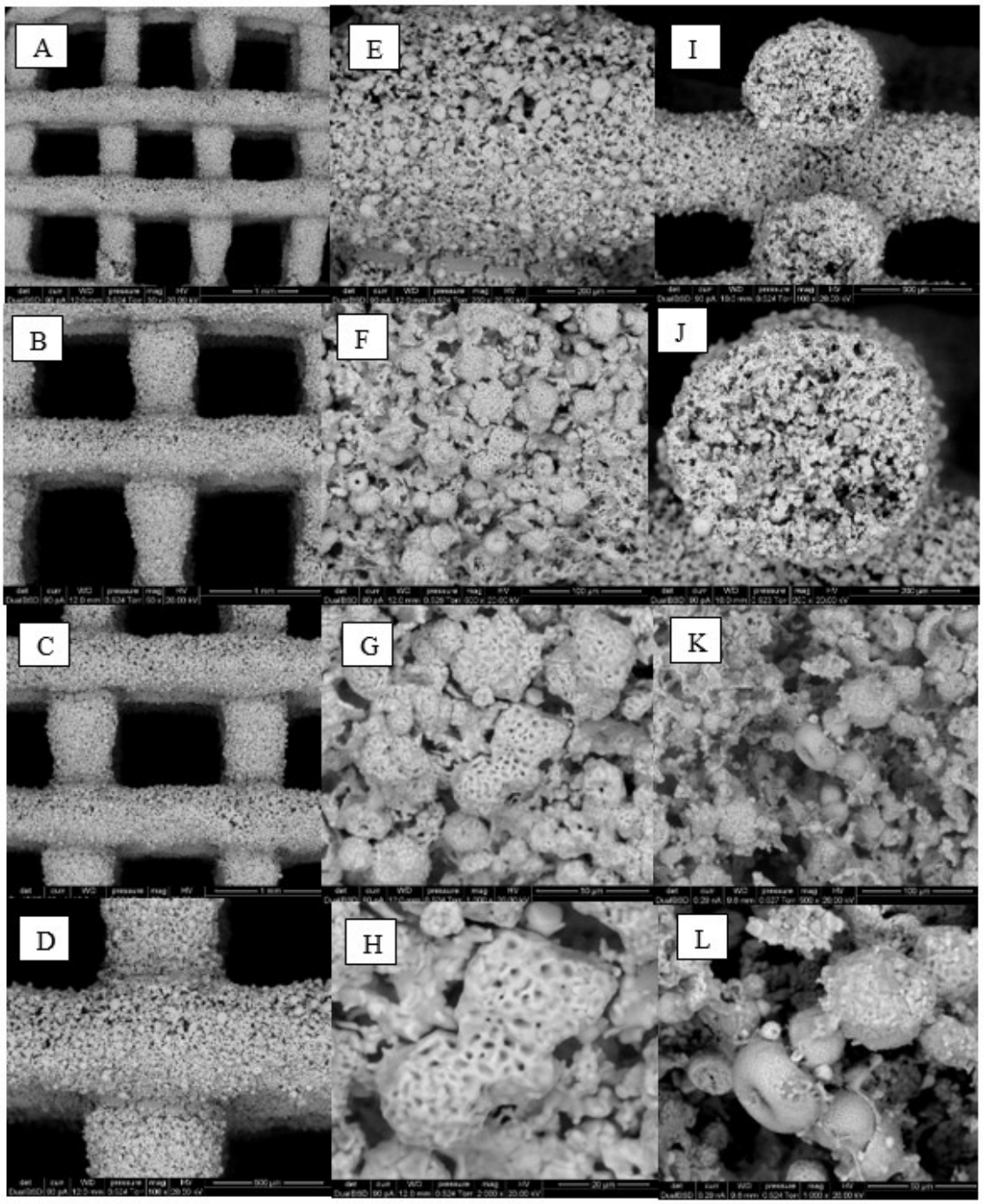

Figure 61: SEM analysis. A-C: Different enlargements show the pattern of the scaffold with detail of the junction between two filaments; (E-H): different magnifications of the same portion of filament; (I-L): Several magnifications of a filament in section

Chapter 6

Conclusions

Direct Ink Writing was used to produce sphene scaffolds for tissue engineering. The two mixtures tested gave very different results in terms of composition.

The ink obtained from calcite nanoparticles expressed a high degree of purity when heat-treated at 1350°C, but unfortunately the printability of the scaffold could not be improved.

The ink obtained from calcium nitrate tetrahydrate salts, on the other hand, exhibited good printability from the outset, but attempts to improve the crystalline phases did not yield good results. Despite this, however, the biocompatibility of the material was maintained and indeed, the presence of phases such as cristobalite (SiO_2) and calcium titanate ($CaTiO_3$) allows the material to improve osteointegrative and osteoinductive properties at the expense of mechanical properties.

In fact, silicon dioxide can promote cell adhesion and bone formation by releasing ions useful for cell metabolism.

Calcium titanate is known for its piezoelectric properties, which can be useful in bone regeneration. These piezoelectric materials can generate electrical charges under mechanical stress, stimulating cell activity and promoting bone cell proliferation and differentiation.

Despite the poor mechanical properties and obvious fragility revealed by compression tests, mechanical characterisation of calcium nitrate tetrahydrate scaffolds in terms of porosity confirmed the presence of a cellular structure reminiscent of spongy bone trabeculae.

Heat treatment at 1350°C was tried but the material was not stable enough and melted.

The use of an inert refractory, e.g. platinum, could be the solution to reach temperatures above 1300°C without compromising and damaging the scaffold.

Despite the efficacy demonstrated in the laboratory, clinical application requires further investigation to assess long-term biocompatibility and resistance under complex physiological conditions.

Future research could focus on in vivo clinical studies to validate the preliminary results obtained in vitro and investigate the long-term integration of scaffolds into human tissues.

In conclusion, this research represents a further step towards the development of innovative materials for regenerative medicine, contributing to the creation of more effective and safer solutions for patients.

Bibliography

1. Boskey, A. L. (2013). Bone composition: relationship to bone fragility and antiosteoporotic drug effects. *Bone*, 53(1), 131-136.
2. Fratzl, P., & Weinkamer, R. (2007). Nature's hierarchical materials. *Progress in Materials Science*, 52(8), 1263-1334.
3. Bonewald, L. F. (2011). The amazing osteocyte. *Journal of Bone and Mineral Research*, 26(2), 229-238.
4. Marie, P. J. (2012). Osteoblasts in osteoporosis: Past, present, and future. *Journal of Cellular Biochemistry*, 113(2), 302-307.
5. Teitelbaum, S. L. (2000). Bone resorption by osteoclasts. *Science*, 289(5484), 1504-1508.]
6. Boyle, W. J., Simonet, W. S., & Lacey, D. L. (2003). "Osteoclast differentiation and activation." Nature
7. Martin, T. J., Seeman, E., & Seibel, M. J. (2019). Bone remodeling: New insights, new roles, new therapeutic targets. *Journal of Bone and Mineral Research*, 34(11), 2047-2050.
8. Raggatt, L. J., & Partridge, N. C. (2010). "Cellular and Molecular Mechanisms of Bone Remodeling." The Journal of Biological Chemistry.
9. Teitelbaum, S. L. (2000). Bone resorption by osteoclasts. *Science*, 289(5484), 1504-1508.
10. Frost, H. M. (2004). A 2003 update of bone physiology and Wolff's Law for clinicians. *The Angle Orthodontist*, 74(1), 3-15.
11. Bonewald, L.F. (2007), Osteocytes as Dynamic Multifunctional Cells. Annals of the New York Academy of Sciences, 1116: 281-290.
12. Qin, L., Bergenstock, Parathyroid Hormone Stimulates Osteoblastic Expression of MCP-1 to Recruit and Increase the Fusion of Pre/Osteoclasts, Journal of Biological Chemistry, Volume 282, Issue 45, 33098 – 33106
13. Parfitt, A. M. (1994). "The Bone Remodeling Space: A Cellular Homestatic System." Journal of Bone and Mineral Research
14. Martin, T. J., & Sims, N. A. (2005). "Osteoclast-derived activity in the coupling of bone formation to resorption." Trends in Molecular Medicine.
15. Seeman, E., & Delmas, P. D. (2006). "Bone Quality—The Material and Structural Basis of Bone Strength and Fragility." New England Journal of Medicine.

16. Väänänen, H. K. (2005). "Mechanism of Osteoclast Mediated Bone Resorption—Rationale for the Design of New Therapeutics." Advanced Drug Delivery Reviews.
17. Wolff, J. (1892). "Das Gesetz der Transformation der Knochen." A. Hirschwald, Berlin.
18. Frost, H. M. (2004). *A 2003 update of bone physiology and Wolff's Law for clinicians.* The Angle Orthodontist, 74(1), 3-15.
19. Turner, C. H., Robling, A. G. (2003). *Mechanical loading and bone formation.* Bone, 31(5), 333-338.
20. Currey, J. D. (2002). *Bones: Structure and Mechanics.* Princeton University Press.
21. Rho, J. Y., Ashman, R. B., & Turner, C. H. (1998). Young's modulus of trabecular and cortical bone material: Ultrasonic and microtensile measurements. *Journal of Biomechanics*, 26(2), 111-119.
22. Zhao, C., Li, H., Han, Q., Zhao, Z., Chen, J., & Wang, X. (2019). Viscoelasticity and tension-compression nonlinearity of trabecular bone in response to different loading rates. *Journal of the Mechanical Behavior of Biomedical Materials*, 98, 150-158.
23. Akkus, O., & Rho, J. Y. (2005). Anisotropic elastic properties of cortical and trabecular bone. *Journal of Orthopaedic Research*, 23(4), 1043-1049.
24. Fontanella Chiara Giulia, Lectures of Meccanica die Biomateriali
25. Ratner, B. D., Hoffman, A. S., Schoen, F. J., & Lemons, J. E. (2013). *Biomaterials Science: An Introduction to Materials in Medicine*. Academic Press.
26. O'Brien, F. J. (2011). Biomaterials & scaffolds for tissue engineering. *Materials Today*, 14(3), 88-95.
27. Todros, S.; Todesco, M.; Bagno, A. Biomaterials and Their Biomedical Applications: From Replacement to Regeneration. *Processes* 2021, *9*, 1949.
28. Bagno A, Lectures from Biomateriali
29. Bagno A, Lectures from Organi Artificiali
30. Williams, D. F. (2009). On the nature of biomaterials. Biomaterials, 30(30), 5897-5909
31. Hench, L. L., & Polak, J. M. (2002). Third-generation biomedical materials. Science, 295(5557), 1014-1017
32. Bellucci, D. Materiali per la vita. Le incredibili storie dei biomateriali che riparano il nostro corpo, Torino, 2022
33. Bernardo, Lectures from Tecnologia dei Biomateriali
34. Todros, S, Lectures from Meccanica dei Biomateriali

35. Elsayed, Hamada & Sayed, Mona & Naga, Salma & Rebesan, Pietro & Gardin, Chiara & Zavan, Barbara & Colombo, Paolo & Bernardo, Enrico. (2021). Additive Manufacturing and Direct Synthesis of Sphene Ceramic Scaffolds from a Silicone Resin and Reactive Fillers. Journal of the European Ceramic Society. 42. 10.1016/j.jeurceramsoc.2021.10.001. C. Wu (2008). Incorporation of titanium into calcium silicate improved their chemical stability and biological properties, J. Biomed. Mater. Res. A 86 (2008) 402–410.
36. M. Muthuraman (1994). Synthesis, properties, sintering and microstructure of sphene, CaTiSiO5: a comparative study of coprecipitation, sol–gel and combustion processes, Mater. Res. Bull. 33 (4) (1998) 655–661.
37. M. Muthuraman (2009). Combustion synthesis of oxide materials for nuclear waste immobilization, Bull. Mater. Sci. 17 (1994) 977.
38. T.S. Lyubenova, (2009). Synthesis of Cr-doped CaTiSiO 5 (2009) 918–924.
39.] J. Panti´ (2013). Influence of mechanical activation on sphene based ceramic material synthesis, Ceram. Int. 39 483–488.
40. C. Wu (2009). Plasma-sprayed CaTiSiO ceramic coating on Ti–6Al–4V with excellent bonding strength, stability and cellular bioactivity, J. R. Soc. Interface 31 (2009) 159–168.
41. C. Wu, Y. Ramaswamy (2009). Novel sphene coatings on Ti–6Al–4V for orthopedic implants using sol–gel method, Acta Biomater. 4 (2008) 569–576.
42. S. Cheng, D. Wei, Y. Zhou, Formation and structure of sphene/titania composite coatings on titanium formed by a hybrid technique of microarc oxidation and heat treatment, Appl. Surf. Sci. 257 (2011) 3404–3411.
43. L. Biasetto, R. Bertolini, H. Elsayed, A. Ghiotti, S. Bruschi, Use of cryogenic machining to improve the adhesion of sphene bioceramic coatings on titanium substrates for dental and orthopaedic applications, Ceram. Int. 45 (2019) 5941–5951.
44. H. Elsayed, G. Brunello, C. Gardin, L. Ferroni, D. Badocco, P. Pastore, S. Sivolella, B. Zavan, L. Biasetto, Bioactive sphene-based ceramic coatings on cpTi substrates for dental implants: an in vitro study, Materials 11 (2018) 2234.
45. H. Elsayed, M. Secco, F. Zorzi, K. Schuhladen, R. Detsch, A.R. Boccaccini, E. Bernardo, Highly porous polymer-derived bioceramics based on a complex hardystonite solid solution, Materials 12 (2019) 3970.
46. A. Zocca, G. Franchin, H. Elsayed, E. Gioffredi, E. Bernardo, P. Colombo, Direct ink writing of a preceramic polymer and fillers to produce hardystonite (Ca 2 ZnSi 2 O 7) bioceramic scaffolds, J. Am. Ceram. Soc. 99 (2016) 1960–1967.

47. H. Elsayed, P. Colombo, E. Bernardo, Direct ink writing of wollastonite-diopside glass-ceramic scaffolds from a silicone resin and engineered fillers, J. Eur. Ceram. Soc. 37 (2017) 4187–4195. Ortona, A. Materiali Ceramici
49. Smith, J. R., & Lee, P. (2018). *Bio-ceramics and their Clinical Applications*. Woodhead Publishing.
50. Hench, L. L. (1998). Bio-ceramics: From Concept to Clinic. *Journal of the American Ceramic Society*, 81(7), 1705-1728.
51. Koch, C. C. (1993). *Mechanical Milling and Alloying*. Butterworth-Heinemann.
52. Rao, P. K., & Jagannath, P. (2015). Synthesis of Hydroxyapatite Nanoparticles by Spray Drying Technique. *Materials Today: Proceedings*, 2(4-5), 3141-3147.
53. Rahaman, M. N. (2007). *Ceramics for biomedical applications*. CRC Press.
54. Fierz, M., et al. (2008). "Evaluation of uniaxial dry pressing of ceramic powders: Theory and experiments." *Journal of the European Ceramic Society*.
55. Bocchini, S., et al. (2014). "Dry pressing of bio-ceramic materials: Optimization and applications." *Journal of Ceramic Processing Research*.
56. Fu, Q., Saiz, E., & Tomsia, A. P. (2011). "Cold isostatic pressing of bio-ceramic scaffolds." *Acta Biomaterialia*.
57. Liu, X., & Ding, C. (2002). "Effect of particle size distribution on the microstructure of bio-ceramic components." *Journal of Biomedical Materials Research*.
58. German, R. M. (1990). *Powder Injection Molding*. Metal Powder Industries Federation.
59. Bose, S., et al. (2013). "Injection molding of bio-ceramics: Process optimization and applications." *Journal of Materials Science: Materials in Medicine*.
60. Fierz, M., et al. (2008). "Binder removal in injection-molded bio-ceramic parts: Optimization and challenges." *Journal of the European Ceramic Society*.
61. Atwood, R. C., et al. (2004). "Automation and cost reduction in bio-ceramic injection molding." *Journal of Manufacturing Science and Engineering*.
62. Zhang, Y., et al. (2017). "Stereolithography of ceramic structures: A review." *Materials Science and Engineering: C*.
63. Mendez, J. A., et al. (2018). "Stereolithography: A rapid prototyping technique for bio-ceramic applications." *Materials Today*.
64. Garcia, M. D., et al. (2019). "Properties of SLA-fabricated bio-ceramic scaffolds for bone tissue engineering." *Advanced Healthcare Materials*.
65. Chen, Y., et al. (2021). "Additive manufacturing of bioactive scaffolds: A review." *Journal of Biomedical Materials Research (52)*

66. Jackson, S. A., & Lee, B. J. (2009). "Lost-wax casting in bio-ceramics: Techniques and innovations." *Advanced Materials Research*.
67. Lichte, P., et al. (2012). "Precision of bio-ceramic components fabricated by lost-wax casting techniques." *Journal of Dental Research*.
68. Lewis, J. A. (2006). "Direct ink writing of 3D functional materials." *Advanced Functional Materials*.
69. Smay, J. E., et al. (2002). "Colloidal inks for directed assembly of 3-D periodic structures." *Journal of the American Ceramic Society*.
70. Li, S., et al. (2019). "Direct ink writing of 3D bio-ceramic scaffolds with complex architectures." *Journal of Materials Science*.
71. Murphy, S. V., & Atala, A. (2014). "3D bioprinting of tissues and organs." *Nature Biotechnology*.
72. Gao, B., et al. (2018). "Direct ink writing based 3D printing of functional materials." *Advanced Materials*.
73. Jones, J. R. (2013). "Review of bioactive glass: From Hench to hybrids." *Acta Biomaterialia*.
74. Wirth, C., et al. (2017). "3D printing of bio-ceramic scaffolds: From fundamental aspects to applications." *Journal of Materials Research*.
75. Nygren, M., & Shen, Z. (2003). "Controlling the pressure and temperature in ceramic sintering processes." *Advanced Materials*.
76. Brinker, C. J., & Scherer, G. W. (2013). *Sol-Gel Science: The Physics and Chemistry of Sol-Gel Processing*. Academic Press.
77. Ashby, M.F. Engineering Materials 2, Pergamon Press, Oxford (UK) 1986. (64)
78. Smith, W.F Scienza e tecnologia dei materiali, McGraw-Hill, Milano 1995.
79. Guglielmi, M Dispense di Scienza e Tecnologia dei Materiali Ceramici (per il Corso di Laurea in Ingegneria dei Materiali)", Biblioteca Centrale di Ingegneria, Padova 2002.
80. Mills, N. J. (2007). *Polymer foams handbook: Engineering and biomechanics applications and design guide*. Butterworth-Heinemann.
81. Banhart, J. (2001). *Manufacture, characterisation and application of cellular metals and metal foams*. Progress in Materials Science, 46(6), 559-632. (68)
82. Wysocki, B., Idaszek, J., Święszkowski, W., Buhagiar, J., & Wierzchoń, T. (2018). Titanium foams for biomedical applications. *Journal of Materials Engineering and Performance*, 27, 1062–1073.

83. Ngo, T. D., Kashani, A., Imbalzano, G., Nguyen, K. T. Q., & Hui, D. (2018). Additive manufacturing (3D printing): A review of materials, methods, applications and challenges. *Composites Part B: Engineering*, 143, 172-196. (70)
84. Gibson, L. J., & Ashby, M. F. (1999). *Cellular solids: Structure and properties* (2nd ed.). Cambridge University Press.
85. Ashby, M. F., Evans, A. G., Fleck, N. A., Hutchinson, J. W., Wadley, H. N., & Gibson, L. J. (2000). *Metal foams: A design guide*. Butterworth-Heinemann.

Sitography

(1) https://www.wacker.com/h/en-us/silicone-resins/silicone-resins/silres-h44/

(2) http://www.inframat.com/products/22N-0811R.htm

(3) https://us.vwr.com/store/category/calcium-nitrate-tetrahydrate

(4) https://funtodo.eu/

(5) https://industriebitossi.com/

(6) https://www.sigmaaldrich.com/IT/it/substance/hexane

(7) https://www.argo-lab.com/overhead-stirrer-/22005013/am-20-d-argolab-overhead-stirrer

(8) https://www.thinkymixer.com/en-gl/product/arm-310/

(9) https://www.3dwasp.com/stampante-3d-delta-delta-wasp-2040-pro

(10) https://help.prusa3d.com/it/tag/cw1

(11) https://www.zeiss.com/microscopy/us/products/light-microscopes

(12) https://www.thermofisher.com

(13) https://www.bruker.com/en/products-and-solutions/diffractometers-and-x-ray

(14) https://www.crystalimpact.de/Default.htm

(15) https://www.anton-paar.com/it-it/prodotti/dettagli/ultrapyc/

(16) https://www.galdabini.it/datasheets/quasar-25

(17) https://www.tersid.it/

Sources of Images and Tables

i. Fontanella Chiara Giulia, Lectures of Meccanica die Biomateriali

ii. https://www.chimica-online.it/biologia/osteociti.htm

iii. https://www.chimica-online.it/biologia/tessuto-osseo-compatto.htm

iv. Raggatt, L. J., & Partridge, N. C. (2010). "Cellular and Molecular Mechanisms of Bone Remodeling." The Journal of Biological Chemistry.

v. Federica Caselli University of Rome “Tor Vergata” Biomechanics of Bone Adaptation A.A. 2012/2013

vi. (17)https://it.m.wikipedia.org/wiki/File:Stress_Strain_Ductile_Material.png

vii. Sadeghian Dehkord E, Kerckhofs G, Compère P, Lambert F, Geris L. An Empirical Model Linking Physico-Chemical Biomaterial Characteristics to Intra-Oral Bone Formation. *Journal of Functional Biomaterials*. 2023; 14(7):388. https://doi.org/10.3390/jfb14070388

viii. Reddy, P.G., Saklani, R., Mandal, M.K., Domb, A.J. (2023). Introduction to Biomaterials. In: Domb, A., Mizrahi, B., Farah, S. (eds) Biomaterials and Biopolymers AAPS Introductions in the Pharmaceutical Sciences, vol 7. Springer, Cham. https://doi.org/10.1007/978-3-031-36135-7_1

ix. Todros, S, Lectures from Meccanica dei Biomateriali

x. Elsayed, Hamada & Sayed, Mona & Naga, Salma & Rebesan, Pietro & Gardin, Chiara & Zavan, Barbara & Colombo, Paolo & Bernardo, Enrico. (2021). Additive Manufacturing and Direct Synthesis of Sphene Ceramic Scaffolds from a Silicone Resin and Reactive Fillers. Journal of the European Ceramic Society. 10.1016/j.jeurceramsoc.2021.10.001.

xi. Smith, J. R., & Lee, P. (2018). *Bio-ceramics and their Clinical Applications*. Woodhead Publishing.

xii. Zhu, RB., Zou, JP., Mao, J. *et al.* A comparison between novel $Gd_2Zr_2O_7$ and $Gd_2Zr_2O_7$/YSZ thermal barrier coatings fabricated by plasma spray-physical vapor deposition. *Rare Met.* **40**, 2244–2253 (2021). https://doi.org/10.1007/s12598-020-01534-x

xiii. Martin Trunec, Karel Maca,Chapter 7 - Advanced Ceramic Processes, Advanced Ceramics for Dentistry (2014) Pages 123-150, https://doi.org/10.1016/B978-0-12-394619-5.00007-9.

xiv. Kustas, A.B., Susan, D.F. & Monson, T. Emerging Opportunities in Manufacturing Bulk Soft-Magnetic Alloys for Energy Applications: A Review. *JOM* **74**, 1306–1328 (2022). https://doi.org/10.1007/s11837-021-05019-9

xv. https://www.researchgate.net/figure/Both-A-continuous-digital-light-processing-cDLP-and-B-stereolithography-SLA_fig1_259766072

xvi. https://www.researchgate.net/figure/Schematic-of-DIW-process-Adapted-with-permission-from-Farahani-et-al-31-Copyright_fig2_347472806

xvii. https://www.argo-lab.com/overhead-stirrer-/22005013/am-20-d-argolab-overhead-stirrer

xviii. https://www.thinkymixer.com/en-gl/product/arm-310/

xix. https://www.3dwasp.com/stampante-3d-delta-delta-wasp-2040-pro

xx. https://help.prusa3d.com/it/tag/cw1

xxi. https://www.zeiss.com/microscopy/us/products/light-microscopes

xxii. https://www.thermofisher.com

xxiii. https://www.bruker.com/en/products-and-solutions/diffractometers-and-x-ray

xxiv. https://www.anton-paar.com/it-it/prodotti/dettagli/ultrapyc/

xxv. https://www.galdabini.it/datasheets/quasar-25

xxvi. https://www.tersid.it/

xxvii. https://www.wacker.com/h/en-us/silicone-resins/silicone-resins/silres-h44/

xxviii. R. Goodall,10 - Porous metals: foams and sponges,In Woodhead Publishing Series in Metals and Surface Engineering,Advances in Powder Metallurgy,Woodhead Publishing,2013,Pages 273-307,ISBN 9780857094209

xxix. https://www.researchgate.net/figure/Elastic-buckling-in-the-cell-walls-a-the-formation-of-plastic-hinges-b-and-cell-wall_fig2_238581027